

Core polarization in inelastic scattering*

F. Petrovich[†]

Lawrence Berkeley Laboratory, University of California, Berkeley, California 94720

H. McManus, J. Borysowicz, and G. R. Hammerstein

Cyclotron Laboratory and Physics Department, Michigan State University, East Lansing, Michigan 48823

(Received 24 November 1976)

Inelastic scattering is a source of much useful information about core polarization effects in nuclei near closed shells. Although there have been many theoretical treatments of core polarization effects reported in the literature, the results of these calculations have rarely been applied to the interpretation of inelastic scattering data. In the present paper we review the microscopic models for the treatment of inelastic proton and electron scattering and the microscopic models for the treatment of core polarization. Estimates are made of core excited admixtures in the wave functions for low-lying states in ^{42}Ca , ^{50}Ti , ^{89}Y , ^{90}Zr , ^{207}Pb , and ^{209}Bi . The resulting wave functions are used to calculate theoretical (p, p') cross sections and (e, e') form factors for comparison with available experimental data. "Realistic" G matrix interactions are used as the starting point in both the structure and the (p, p') calculations. In the structure calculations the interaction is modified by means of a "bootstrap" prescription to account for important long-range core correlations and in the (p, p') calculations it is modified by the addition of an imaginary component. It is concluded that the overall features of the experimental data can be understood from these calculations.

[NUCLEAR STRUCTURE, NUCLEAR REACTIONS (p, p') and (e, e') ; nuclei near closed shells; microscopic model for core polarization; calculated $\sigma(\theta)$ and $F(q)$.]

I. INTRODUCTION

The concept of core polarization is quite well known in the shell model interpretation of nuclei in the vicinity of closed shells. In the shell model a nuclear state is described in a restricted configuration space which presumably contains the bulk of its wave function, but not all its significant components. This restricted configuration space, commonly called the model space, usually consists of a few valence particles (holes) distributed among a small number of shell model orbitals outside (inside) an inert closed shell core. The term core polarization is generally associated with effects which are due to wave function admixtures not in the model space. The name arises because these admixtures most often will consist of core-excited configurations. Core polarization can be taken into account by defining effective operators in the model space which may be calculated by means of perturbation theory.

These ideas first appeared in the literature about 20 years ago^{1,2} when it was first noted that there were discrepancies between the predictions of the simple shell model and the experimental values for nuclear magnetic moments, quadrupole moments, γ -transition rates, etc. Two different models were proposed at this time. One is a hybrid model in which the core is treated as a liquid drop which can be set into oscillation by interaction with the extracore nucleons.¹ The other is a

completely microscopic model² in which the core is considered to be an assemblage of nucleons—any of which might be raised to higher, unoccupied levels as a result of the two-body forces which couple them to the valence nucleons.

In recent times this microscopic model has been pursued in considerably greater depth. The major impetus here has been the work of Brown and collaborators³⁻⁸ whose purpose was to gain an understanding of the properties of finite nuclei using "realistic" forces, i.e., interactions which can be derived directly from the free two-nucleon potential. As the nucleon-nucleon interaction is strong and singular, the first step in this approach is to truncate to a large shell model basis by applying Brueckner Hartree-Fock theory to get rid of the short range two-nucleon correlations and replace the singular interaction by a smooth well-behaved one, namely, the bare G matrix. The second step is to truncate to the model space and to renormalize the bare G matrix to account for core polarization as described in the first paragraph above. The renormalized G matrix is the shell model effective interaction.

Kuo and Brown^{4,8} have made a systematic study of nuclei with ^{16}O , ^{40}Ca , ^{48}Ca , ^{56}Ni , ^{88}Sr , and ^{208}Pb cores using second order perturbation theory in renormalizing the bare G matrix. They find that core polarization gives rise to a strong pairing effect which is the major feature of the observed spectra. Although the results of these

calculations are quite impressive, attempts⁹ to extend the perturbative treatment to higher orders have not met with the same success and the final status of core polarization and the effective interaction is still an open question. A similar situation prevails in regard to associated efforts¹⁰ to calculate nuclear magnetic moments, quadrupole moments, and quadrupole transition rates. Lowest order perturbation theory provides a reasonable qualitative estimate of these effects, but there are still many ambiguities in the interpretation of the results of calculations which include higher order contributions. Much of this work has been reviewed recently by Barrett and Kirson.¹¹

The purpose of the present paper is to present the results of calculations, similar to those of Ref. 10, but applied to the problem of inelastic scattering. In particular, we consider inelastic electron scattering and inelastic proton scattering. Inelastic proton scattering at energies below 100 MeV is interesting, because the interaction between the incident proton and the bound nucleons is quite similar to the interaction between bound nucleons, i.e., the bare G matrix.^{12,13} Electron scattering is primarily sensitive to proton excitations in the target nucleus while proton scattering is most sensitive to neutron excitations.¹⁴ By comparing results for these two reactions a measure of both the proton and neutron components of the nuclear wave functions is obtained. In addition, inelastic scattering provides information about core polarization effects in transitions requiring large angular momentum transfer. Cross sections have been measured for transitions where there are up to 11 units of angular momentum transferred. This is to be contrasted with low momentum electromagnetic data which are essentially restricted to dipole, quadrupole, and some octupole phenomena.

The first attempt at treating core polarization in inelastic proton scattering was made by Love and Satchler.¹⁵ They assume a hydrodynamical description of the core and showed that core polarization can give a large, even dominant, contribution to the cross section. The main purpose of the present paper is to show that the major features of inelastic scattering from nuclei near closed shells can be qualitatively understood in completely microscopic calculations based on realistic interactions. In the calculations, core excited admixtures in the nuclear wave functions are estimated using lowest order perturbation theory and a "bootstrap" prescription which accounts for long-range core correlations. Agassi and Schaeffer¹⁶ have previously made a similar but considerably more limited study of these same

effects. We also note that some results obtained with wave functions from the present paper have previously been reported elsewhere.^{17,18}

In the next section of this paper we give a brief description of the theoretical treatment of inelastic proton and inelastic electron scattering. We review the theory of effective operators and describe our calculations in Sec. III. The results of the calculations are discussed in Sec. IV and Sec. V contains the conclusions.

II. INELASTIC SCATTERING

A. Inelastic proton scattering

1. Microscopic model

In the microscopic model proton-nucleus scattering is described in terms of a projectile-target interaction which has the form

$$V = \sum_i t_{ip}, \quad (1)$$

where t_{ip} is a two-body force acting between the projectile and the i th target nucleon. The two-body force t_{ip} has both real and imaginary parts, because, even in the most elaborate of reaction calculations, only a few of the allowed channels are treated explicitly. In principle, t_{ip} can be derived directly from the free two-nucleon potential. Such a calculation is not easy; however, as it requires the treatment of the repulsive hard cores which appear in the free two-nucleon potential combined with an explicit treatment of the excluded reaction channels.

Although a program of this type has not been carried out in detail, a reasonable prescription for t_{ip} , applicable in the energy region below 100 MeV, has been developed in recent years.^{12,13} It is based on the assumptions that the real part of t_{ip} is not too different from the bound state G matrix and that the effects of the excluded reaction channels can be estimated perturbatively or treated phenomenologically. The first assumption has been tested in several calculations.¹²⁻¹⁴ Attempts to estimate the effect of the excluded reaction channels have, so far, been restricted to the case of elastic scattering.^{12,19} Satchler has proposed a method²⁰ whereby the imaginary part of t_{ip} for inelastic scattering calculations can be inferred from the imaginary part of the phenomenological optical potential for elastic scattering. This method has proved to be useful in several calculations.^{13,18,20,21} Additional comments concerning this prescription for t_{ip} may be found in Ref. 13.

Another problem which is encountered in any attempt to treat proton-nucleus scattering in a microscopic model is the indistinguishability of

the incident proton and the target nucleons. In this situation the Pauli principle requires that the wave function for the projectile-target system be completely antisymmetrized—which in turn gives rise to “knock-on” exchange amplitudes in the transition matrix elements. These are nonlocal in the projectile coordinate and they are quite important, particularly in the case of inelastic transitions.^{22,23,12,13} Computer codes are available which allow the inclusion of these exchange amplitudes and their properties have been studied in some detail.^{13,22,23} In this work we include these terms with a zero-range approximation developed previously.^{12,24}

2. Interaction

In the present calculations we assume t_{i_p} to be given by

$$t_{i_p} = t_{i_p}^R + i t_{i_p}^I, \quad (2)$$

where R and I denote real and imaginary, respectively.

We take $t_{i_p}^R$ to be the long-range part of the Hamada-Johnston (HJ) potential^{25,4,5,12,13} with the closure approximation to the second order tensor contribution. We assume a 1.05 fm separation distance and a closure energy denominator of 220 MeV. This is a local, even state central interaction which can be written

$$t_{i_p}^R = g_{i_p}^0 = g_{\rho q}^0(r_{i_p}) + g_{\rho q}^1(r_{i_p}) \vec{\sigma}_i \cdot \vec{\sigma}_p \quad (3)$$

with $q = p$ or n as i is a proton or neutron. The expression for the radial functions appearing in Eq. (3) have been given elsewhere^{4,5,12,13} and will not be repeated here. For orientation we note that

$$g_{pn}^0 \approx 3g_{pp}^0 \approx 9g_{pn}^1 \approx -3g_{pp}^1 \quad (4)$$

with all components but g_{pp}^1 being attractive.

We neglect the central interaction in odd states. This has been included in some calculations by fitting a regular functional form to the low energy nucleon-nucleon P -wave phase shifts^{12,13} and its effect is not large. We do not include possible spin-orbit and tensor components in $t_{i_p}^R$. The properties of these noncentral interaction components have been discussed in detail elsewhere^{26,27} and are only of secondary importance for most of the transitions considered in this paper.

For $t_{i_p}^I$ we follow Ref. 20 and argue that the imaginary part of the optical potential for elastic scattering is given by

$$U_I(r_p) = \langle \text{g.s.} | \sum_i t_{i_p}^I | \text{g.s.} \rangle + \text{exchange terms.} \quad (5)$$

With the assumption that

$$t_{i_p}^I = A_{pq}(r_i) \delta(\vec{r}_i - \vec{r}_p) \quad (q = p, n) \quad (6)$$

the two terms on the right of Eq. (5) are equal and

$$U_I(r_p) = 2A_{pp}(r_p)\rho_p(r_p) + 2A_{pn}(r_p)\rho_n(r_p), \quad (7)$$

where ρ_p and ρ_n are the ground state proton and neutron density functions. With the additional assumption that

$$\rho_n = (N/Z)\rho_p, \quad (8)$$

we obtain

$$U_I(r_p) = A(r_p)\rho_p(r_p), \quad (9)$$

$$A = 2[A_{pp} + (N/Z)A_{pn}].$$

A can be determined by comparing directly U_I and ρ_p which are available from phenomenological analyses of elastic proton and electron scattering data. As A_{pp} and A_{pn} cannot be determined separately from the data, we make the *ansatz* that A_{pp} and A_{pn} have the same radial shape and that their strengths are in the same ratio as the volume integrals of the corresponding components of $t_{i_p}^R$, i.e.,

$$A_{pn} = \alpha A_{pp}. \quad (10)$$

For the long-range part of the HJ potential $\alpha = 2.58$.¹²

In the above paragraph it has been assumed that the imaginary part of the projectile-target interaction for inelastic scattering is proportional to that for elastic scattering. It has been argued²⁸ that the various excluded channels contribute coherently to the imaginary part of the optical potential for elastic scattering, but that the separate contributions interfere to some degree in the case of an inelastic excitation. This means that $t_{i_p}^I$ for elastic scattering should be greater than $t_{i_p}^I$ for inelastic scattering. With this argument in mind we simply point out that the prescription outlined above gives, in all probability, an upper limit on $t_{i_p}^I$ for inelastic transitions. We also mention that the assumption that $\alpha = 2.58$ in Eq. (10) is tantamount to assuming that excluded channels which favor neutron excitation, e.g., (p, p') and (p, d) , are more important than those which favor proton excitation, e.g., $(p, 2p)$. Although this does not seem unreasonable, this point has not been investigated in detail and could, in fact, be wrong. Fortunately, the results to be presented are not critically dependent on this assumption.

3. Distorted wave approximation

The differential cross section for inelastic proton scattering can be written as follows

$$\frac{d\sigma}{d\Omega} = \left(\frac{\mu}{2\pi\hbar^2} \right)^2 \frac{k_f}{k_i} \frac{1}{2(2J_i + 1)} \sum |T_{fi}|^2, \quad (11)$$

where μ is the reduced mass of the projectile-tar-

get system, k_f and k_i are the final and initial relative wave numbers, J_i is the initial spin of the target, T_{fi} is the transition amplitude, and the sum is over the initial and final projections of the projectile and target. In the distorted wave approximation the transition amplitude is given by

$$T_{fi} = \int \chi_f^{(-)*}(\bar{r}_p) \langle f | V | i \rangle \chi_i^{(+)}(\bar{r}_p) d^3 r_p, \quad (12)$$

+ exchange terms,

where the χ 's are distorted waves and $|i\rangle$ and $|f\rangle$ are the initial and final states of the target. The first term in this equation is the direct amplitude and the second is the knock-on exchange amplitude. With the approximation of Refs. 12 and 24, the exchange terms can be included by replacing V in the first term of Eq. (12) by

$$\bar{V} = \sum_i v_{i_p}, \quad (13)$$

where

$$v_{i_p} = t_{i_p}^R + 2it_{i_p}^I + t_{i_p}^R(k_L^2) \delta(\bar{r}_i - \bar{r}_p). \quad (14)$$

For the imaginary component of V the direct and exchange amplitudes are equal because $t_{i_p}^I$, as defined in Eq. (6), is assumed to be a zero-range interaction. This accounts for the factor of 2 multiplying $t_{i_p}^I$ in Eq. (14). The exchange amplitude corresponding to the real part of V is given by the last term in Eq. (14) where $t_{i_p}^R(k_L^2)$ is the Fourier transform of $t_{i_p}^R$ evaluated at the wave number associated with the laboratory energy of the incident proton.

To understand this approximation it is sufficient to consider the scattering of a free nucleon from another nucleon bound in a fixed potential well. On the average the bound nucleon is at rest with respect to the incident nucleon. In order for the incident nucleon to knock out the bound nucleon and be captured in the potential well it is necessary that it impart all its momentum to the bound nucleon. This is a very high energy argument in that we ignore the spread of momentum components in the wave function for the bound nucleon as well as the effect of the binding potential; however, in practice it is found to work quite well¹² even for energies below 100 MeV.

Noting that $t_{i_p}^R$ and $t_{i_p}^R(k_L^2)$ have essentially the same sign, we see that the direct and exchange contributions in Eq. (14) are in phase. This is a direct consequence of the fact that the interaction being considered has only even state components. Exchange amplitudes for odd state interactions are out of phase with the direct amplitudes.^{12,13,22,23} This is a contributing factor in allowing us to neglect the odd state components of the projectile-target interaction.

The essential point of the preceding development is that inelastic proton scattering cross sections can be understood reasonably well in local distorted wave calculations, that is

$$T_{fi} = \int \chi_f^{(-)*}(\bar{r}_p) \langle f | \bar{V} | i \rangle \chi_i^{(+)}(\bar{r}_p) d^3 r_p, \quad (15)$$

where \bar{V} is a pseudopotential, derived from a realistic interaction, which incorporates the major features of knock-on exchange. The relative strengths of the components of \bar{V} are very nearly the same as the relative strengths of the components of the real part of V which have been given in Eq. (4). As we are interested in treating nuclear wave functions which contain many components, the reduction of the calculations to the form of Eq. (15) is important. In this situation an exact treatment of Eq. (12) can be very expensive or, in some cases, impossible to carry out.

The evaluation of the integral in Eq. (15) is straightforward.²⁹ The procedure is to expand \bar{V} in multipoles which correspond to definite orbital, spin, and total angular momentum transfer (LSJ). This expansion is given by

$$\bar{V} = \sum_{\substack{L \\ LSJ \\ M_J}} v_{p,qL}^S(r_p; r_i) (-1)^{J+S+M_J} T_{-M_J}^{LSJ}(p) T_{M_J}^{LSJ}(i), \quad (16)$$

($q = p, n$)

where $v_{p,qL}^S(r_p; r_i)$ is the L th multipole coefficient in the Legendre expansion of $v_{p,q}^S(r_i)$ and $T_{M_J}^{LSJ}$ is the "spin-angle" tensor

$$T_{M_J}^{LSJ} = \sum_{M_\lambda} \langle LSM_\lambda | JM_J \rangle i^L Y_{LM}^S \sigma_\lambda. \quad (17)$$

Inserting Eq. (16) into Eq. (15), performing the integration over the target coordinates and projectile spin coordinates, and carrying out the summations in Eq. (11), we obtain immediately the final expression for the differential cross section:

$$\frac{d\sigma}{d\Omega} = \left(\frac{\mu}{2\pi\hbar^2} \right)^2 \frac{k_f}{k_i} \frac{2J_f+1}{2J_i+1} \sum_{LSJM} |J_{LSJM}^2|, \quad (18)$$

$$\beta_{LSJM}^{LM} = \frac{i^{-L}}{\hat{L}} \int \chi_f^{(-)*}(\bar{r}_p) \bar{F}^{LSJ}(r_p) Y_{LM}^*(\hat{r}_p) \chi_i^{(+)}(\bar{r}_p) d^3 r_p,$$

$$\hat{L} = (2L+1)^{1/2}.$$

We have ignored the effect of spin-orbit coupling in the optical potential in writing Eq. (18) although we do include it in the calculations. It gives rise to interference between amplitudes of the same J with different L and S .²⁹ In practice this interference is found to be weak.

All information pertaining to the projectile-target interaction and the details of nuclear structure

are contained in the radial form factors, $\bar{F}^{LSJ}(r_p)$, which appear in Eq. (18). The nuclear structure information is confined to the radial nuclear transition densities which are defined by

$$F_q^{LSJ}(r) = \left\langle f \left\| \sum_i \frac{\delta(r-r_i)}{r_i^2} T^{LSJ}(i) \right\| i \right\rangle \quad (q=p, n), \quad (19)$$

where $\langle \parallel \rangle$ is a reduced matrix element³⁰ and the sum on i runs over target protons or neutrons as $q=p$ or n . The radial form factors are obtained by averaging \bar{V} over the transition densities, i.e.,

$$\bar{F}^{LSJ}(r_p) = \sum_{q=p, n} \int_0^\infty v_{pqL}^S(r_p; r) F_q^{LSJ}(r) r^2 dr. \quad (20)$$

With the approximations employed here, inelastic proton scattering is simply a one-body operator with respect to the target. This is quite evident from Eqs. (18)–(20). The selection rules for the reaction are contained in Eq. (19). These are:

$$J = \Delta(J_f J_i J), \quad S = \Delta(\frac{1}{2} \frac{1}{2} S), \quad L = \Delta(JS L), \quad (21)$$

$$\Delta\pi = (-1)^L. \quad (22)$$

There is some violation of the parity selection rule, Eq. (22), when exchange is treated exactly.^{13, 22, 23} Although it is possible to include the amplitudes which violate Eq. (22) in an approximate way,²⁴ we ignore them here as they contribute little to the differential cross sections.

We distinguish between normal parity [$\Delta\pi = (-1)^J$] and abnormal parity amplitudes [$\Delta\pi = (-1)^{J+1}$]. In the former case the allowed values of LSJ are $J0J$ and $J1J$ and the reaction can proceed through the strong spin independent components of the projectile-target interaction. Neutron excitations will be most important here as $v_{pn}^0 \approx 3v_{pp}^0$. In the latter case the allowed values of LSJ are $J \pm 11J$ and the reaction can proceed only through the weaker spin dependent parts of the projectile-target interaction. We will see in Sec. III that the effect of core polarization is to enhance the $S=0$ transition densities while retarding the $S=1$ transition densities. For most of the transitions which will be considered in Sec. IV, a single $S=0$ amplitude will make the dominant contribution to the cross section.

B. Inelastic electron scattering

The differential cross section for inelastic electron scattering is given by³¹

$$\frac{d\sigma}{d\Omega} = \frac{Z^2 \sigma_M}{\eta} [|F_L(q)|^2 + \frac{1}{2}(1 + 2 \tan^2 \frac{1}{2} \theta) |F_T(q)|^2], \quad (23)$$

where $Z^2 \sigma_M$ is the Mott cross section which describes the scattering of a high energy electron

by a point charge Z , η is a recoil factor, θ is the scattering angle, and q is the magnitude of the momentum transfer. $F_L(q)$ and $F_T(q)$ are the longitudinal and transverse form factors, respectively. As a result of the difference in the angular dependence of the two terms in Eq. (23), it is possible to determine both $F_L(q)$ and $F_T(q)$ from the experimental data. Since we will consider only cases where $F_L(q)$ is dominant or where $F_L(q)$ has been separated from $F_T(q)$, the following discussion will be confined to the longitudinal form factor. Details concerning the transverse form factor may be found in Ref. 31.

We assume here a Born approximation treatment with a local wave number correction to account for Coulomb distortion.³¹ This approach has been shown to be adequate, even for heavy nuclei, provided we do not require information inside the nuclear surface.¹⁴ With these assumptions the longitudinal form factor is given by

$$|F_L(q)|^2 = \frac{4\pi}{Z^2} \frac{2J_f + 1}{2J_i + 1} \sum_J \left| \int_0^\infty j_J(\kappa q r) \rho_{ch}^J(r) r^2 dr \right|^2. \quad (24)$$

In this equation $j_J(\kappa q r)$ is a spherical Bessel function and the factor κ appearing in its argument defines the local wave number. It is given by^{31, 14}

$$\kappa = 1 - V_C(0)/E, \quad (25)$$

where $V_C(0)$ is the Coulomb potential at the center of the target and E is the energy of the incident electron. In addition $\rho_{ch}^J(r)$ is the radial charge transition density which is obtained by averaging the proton charge distribution³² over the nuclear proton transition density defined in Eq. (19). The averaging integral is

$$\rho_{ch}^J(r) = \int_0^\infty \rho_p^J(r; r') F_p^{J0J}(r') r'^2 dr', \quad (26)$$

where $\rho_p^J(r; r')$ is the J th multipole coefficient in the Legendre expansion of the proton charge distribution. The longitudinal form factor determined by inelastic electron scattering provides a measure of the $S=0$ proton transition density, in contrast to inelastic proton scattering which, when a normal parity amplitude is dominant, is more sensitive to the $S=0$ neutron transition density.

In closing this section we note that the longitudinal electron scattering form factor, in the region of small q , is simply related to the reduced transition probabilities determined in γ -decay measurements. To see this we replace the spherical Bessel function in Eq. (24) by the leading term in its power series which is valid for small argument and note that the averaging integral Eq. (26) conserves the J th moment of $F_p^{J0J}(r)$,³³ i.e.,

$$\int \rho_{\text{ch}}^J(r) r^{J+2} dr = \int F_p^{J_0 J}(r) r^{J+2} dr. \quad (27)$$

We obtain

$$|F_L(q)|^2 = \frac{4\pi}{Z^2} \sum \frac{(\kappa q)^{2J}}{[(2J+1)!!]^2} B(EJ\uparrow), \quad (28)$$

where $B(EJ\uparrow)$ is the reduced transition probability

$$B(EJ\uparrow) = \frac{2J_f + 1}{2J_i + 1} \left| \int_0^\infty F_p^{J_0 J}(r) r^{J+2} dr \right|^2. \quad (29)$$

III. THEORY OF EFFECTIVE OPERATORS

The theory of effective operators is quite well known and has been discussed in many places.^{5-7,11,34} We briefly review it here, following closely a discussion due to Harvey and Khanna,³⁴ in order to provide background for the calculations to be presented.

A. Formal theory

1. Effective Hamiltonian

The nuclear Hamiltonian is generally written

$$H = H_0 + G, \quad (30)$$

where H_0 is an independent particle Hamiltonian

$$H_0 = \sum_i T_i + \sum_i U_i \quad (31)$$

which has both kinetic and potential energy parts and

$$G = \sum_{i < j} g_{ij} \quad (32)$$

is the residual interaction. We assume that the difficulties associated with the hard core in the free two-nucleon potential have already been dealt with, so that g_{ij} is the bare G matrix interaction. It is usual to express the eigenfunction of H in terms of the complete set of states belonging to H_0 ,

$$H|\psi\rangle = E|\psi\rangle, \quad (33)$$

$$|\psi\rangle = \sum_i \alpha_i |\phi_i\rangle, \quad H_0|\phi_i\rangle = \epsilon_i |\phi_i\rangle. \quad (34)$$

Since the set of basis states $\{|\phi_i\rangle\}$ is in general infinite in dimension, it is necessary to truncate to a finite basis in order to perform a practical calculation.

To affect this truncation the projection operators

$$P = \sum_{i \in d} |\phi_i\rangle \langle \phi_i|, \quad (35)$$

$$Q = \sum_{i \in \bar{d}} |\phi_i\rangle \langle \phi_i|$$

are introduced. In the above equation, d denotes the model space and the remaining space is referred to as the excluded space. Introducing the notation

$$|\psi_P\rangle = P|\psi\rangle, \quad |\psi_Q\rangle = Q|\psi\rangle \quad (36)$$

and noting that

$$P^2 = P, \quad Q^2 = Q, \quad QP = PQ = 0, \quad P + Q = 1, \quad (37)$$

$$PH_0Q = QH_0P = 0,$$

it is straightforward to show that

$$\bar{H}|\psi_P\rangle = (H_0 + \bar{G})|\psi_P\rangle = E|\psi_P\rangle, \quad (38)$$

$$\bar{G} = G + G \frac{Q}{E - H_0} \bar{G}, \quad (39)$$

$$|\psi_Q\rangle = \frac{Q}{E - H_0} \bar{G}|\psi_P\rangle, \quad (40)$$

where the problem of diagonalizing H in an infinite basis has been replaced by the problem of diagonalizing an effective Hamiltonian \bar{H} in a finite basis. \bar{G} is the shell model effective interaction.

Equations (38)–(40) are completely equivalent to Eqs. (33)–(34) for those eigenstates of H which have some overlap with the model space. Equation (38) gives the exact eigenvalues as well as the exact model space projection of the wave functions for these states. The components of the wave functions in the excluded space are given by Eq. (40). The claim made in the first of the two preceding sentences may seem surprising, since the number of eigenstates of H which have nonvanishing overlap with the model space surely exceeds the dimensionality of the model space. The solution to this problem comes in noting that \bar{G} (hence \bar{H}) depends upon the exact eigenvalue, so that Eq. (38) is not the usual eigenvalue problem. In practical calculations the energy denominator appearing in the expression for \bar{G} is fixed in some average way. This limits the approach to the treatment of a few eigenstates of H which presumably have a large overlap with the model space.

2. Normalization of eigenfunctions

The normalization of $|\psi_P\rangle$ and $|\psi_Q\rangle$ has not yet been specified. In accord with convention we normalize $|\psi_P\rangle$ to unity so that

$$\langle \psi_P | \bar{H} | \psi_P \rangle = E. \quad (41)$$

The norm of $|\psi_Q\rangle$ is then given by

$$n^2 = \langle \psi | \psi \rangle = \langle \psi_P | \psi_P \rangle + \langle \psi_Q | \psi_Q \rangle. \quad (42)$$

Using Eq. (40) it immediately follows that

$$n^2 = \langle \psi_P | N^2 | \psi_P \rangle$$

$$= \langle \psi_P | 1 + \bar{G} \frac{Q}{(E - H_0)^2} \bar{G} | \psi_P \rangle. \quad (43)$$

With this normalization convention the admixtures of the true wave function in the model space and excluded space are

$$A_P^2 = \frac{1}{n^2} \quad \text{and} \quad A_Q^2 = \frac{n^2 - 1}{n^2}, \quad (44)$$

respectively. If we write

$$|\psi_P\rangle = \sum_i \alpha_i |\phi_i\rangle, \quad (45)$$

then the amplitude of $|\phi_j\rangle$ ($j \in d$) in the true wave function is

$$A_j = \alpha_j / n \quad (j \in d). \quad (46)$$

In addition, we find that the admixture of $|\phi_j\rangle$ ($j \in d$) in the true wave function is

$$A_j = \sum_{i \in d} A_i a_{ji} \quad (j \in d), \quad (47)$$

where

$$a_{ji} = \langle \phi_j | \frac{Q}{E - H_0} \bar{G} | \phi_i \rangle \quad (i \in d, j \in d) \quad (48)$$

is the amplitude of the excluded space configuration $|\phi_j\rangle$ in the model space configuration $|\phi_i\rangle$.

3. Effective transition operators

The transition matrix element of a one-body operator, $\mathcal{T} = \sum_i t_i$, taken between two eigenstates of H , $|\psi^i\rangle$ and $|\psi^f\rangle$, is given by

$$\langle \mathcal{T} \rangle_{fi} = n_i^{-1} n_f^{-1} \langle \psi^f | \mathcal{T} | \psi^i \rangle. \quad (49)$$

The factor $(n_i n_f)^{-1}$ is necessary because the wave functions of H have not been normalized to unity. Just as it is possible to replace the eigenvalue problem for H in an infinite basis by an eigenvalue problem for an effective Hamiltonian in a finite model space, $\langle \mathcal{T} \rangle_{fi}$ can be expressed in terms of the matrix element of an effective, $\bar{\mathcal{T}}$, taken between model space wave functions. The proof is short and serves to define the effective transition operator. We write

$$\langle \mathcal{T} \rangle_{fi} = n_i^{-1} n_f^{-1} \langle \psi^f | (P + Q) \mathcal{T} (P + Q) | \psi^i \rangle. \quad (50)$$

Then we replace $|\psi_Q\rangle$ on the right by its expression in terms of $|\psi_P\rangle$, Eq. (40), to obtain

$$\langle \mathcal{T} \rangle_{fi} = n_i^{-1} n_f^{-1} \langle \psi_P^f | \bar{\mathcal{T}} | \psi_P^i \rangle, \quad (51)$$

where

$$\bar{\mathcal{T}} = \mathcal{T} + \mathcal{T} \frac{Q}{E - H_0} \bar{G} + \bar{G} \frac{Q}{E - H_0} \bar{\mathcal{T}} + \bar{G} \frac{Q}{E - H_0} \mathcal{T} \frac{Q}{E - H_0} \bar{G}. \quad (52)$$

We also note that Eq. (51) can be rewritten as

$$\langle \mathcal{T} \rangle_{fi} = \sum_{i, j \in d} A_i^f A_j^i \langle \phi_i | \bar{\mathcal{T}} | \phi_j \rangle. \quad (53)$$

B. Schematic model and discussion

It is clear from the above development that a complete discussion of the nuclear problem requires only a knowledge of the matrix elements $\langle \phi_i | \bar{G} | \phi_j \rangle$, $\langle \phi_i | N^2 | \phi_i \rangle$, and $\langle \phi_i | \bar{\mathcal{T}} | \phi_j \rangle$ with $(i, j \in d)$. Actual calculation of these matrix elements is not a trivial matter, unfortunately, and even though this problem has received a great deal of attention it has yet to be completely solved.¹¹ Two estimates of the matrix elements of $\bar{\mathcal{T}}$ are made in this work.

For the first estimate we use lowest order perturbation theory. In lowest order \bar{G} , N^2 , and $\bar{\mathcal{T}}$ are approximated by

$$G \approx G + G \frac{Q}{\frac{1}{2}(\epsilon_i + \epsilon_j) - H_0} G, \quad (54)$$

$$N^2 \approx 1, \quad (55)$$

$$\bar{\mathcal{T}} \approx \mathcal{T} + \mathcal{T} \frac{Q}{\epsilon_j - H_0} G + G \frac{Q}{\epsilon_i - H_0} \mathcal{T}, \quad (56)$$

where E has been suitably defined in terms of the eigenvalues of H_0 . This approximation gives a coupling between the model space and the excluded space, but neglects entirely any configuration interaction in the excluded space. The latter is evident from the free propagators which appear in Eqs. (54) and (56).

The low-lying spectra of nuclei which are two particles (2p) or two holes (2h) away from closed shells are reproduced quite well in calculations employing Eq. (54).⁴⁻⁸ The matrix elements of $\delta G = \bar{G} - G$ are strong and attractive in cases of the interaction energy of two identical nucleons coupled to zero total angular momentum with the main contribution coming from 3p-1h or 3h-1p states of energy $2\hbar\omega$. This is the pairing effect mentioned in the Introduction of this paper. Calculations which use Eqs. (55) and (56) (see Ref. 10) provide at best a qualitative estimate of transition matrix elements in nuclei np or nh away from closed shells. The main contribution to $\delta\mathcal{T} = \bar{\mathcal{T}} - \mathcal{T}$ comes from $(n+1)p$ -1h or $(n+1)h$ -1p intermediate states of energy $2\hbar\omega$ and $1\hbar\omega$ for positive and negative parity transitions, respectively. Matrix elements of $\delta\mathcal{T}$ generally have the right sign and are of the correct order of magnitude, although they are typically underestimated. A specific difficulty occurs in effective charge calculations where it is found that polarization charges for valence protons are smaller than for

valence neutrons which is in contradiction to experiment.

Lowest order perturbation theory implies a rather direct relationship between the renormalization of G and \mathcal{T} in the case of states arising from two like nucleons in a (j^2) configuration, i.e., $\frac{1}{2}(2j+1)$ states with $J^\pi = 0^+, 2^+, \dots, (2j-1)^+$. Specifically, pairing occurs as a result of coherent contributions from the coupling between the valence nucleons and core excitations of different multipolarity. On the other hand, transitions starting from the 0^+ state and ending on one of the higher spin states J_f^+ depend only on the coupling between the valence nucleons and core excitations of multipolarity J_f . Inelastic scattering affords an excellent opportunity to study the above relation, since it is the only source of experimental data which gives information on the direct excitation of the higher spin states of these configurations.

To see the above schematically, we make use of the hydrodynamical description of the core and closure which allows us to write analytic expressions for the effective operators in the model space. Considering only coupling between the valence nucleons and normal parity core excitations we find^{1,35}

$$\delta G = - \sum_{\substack{i < j \\ LM}} \theta_L k_v(r_i) k_v(r_j) Y_{LM}^*(\hat{r}_i) Y_{LM}(\hat{r}_j), \quad (57)$$

$$k_v(r) = -R_v \frac{dU(r-R_v)}{dR_v},$$

where the sum on i and j runs only over the valence nucleons, U_v is the potential which binds the valence nucleon to the core, R_v is the radius parameter in this potential, and

$$\theta_L = \frac{1}{C_L} \quad (58)$$

gives the effective strength of the coupling to 2^L -pole core excitations. C_L is the effective core stiffness parameter for 2^L -pole excitations. In a physical nucleus, there are, of course, more than one core excitation of each multipolarity. The reduction of the effect of these core excitations to a single coupling constant is where closure enters this model. In a similar manner, we find the core polarization correction to the projectile-target interaction for the (p, p') reaction to be given by^{15,35}

$$\delta \bar{V} = - \sum_{LM} \theta_L k(r_p) k_v(r_i) Y_{LM}^*(\hat{r}_p) Y_{LM}(\hat{r}_i), \quad (59)$$

where $k(r_p)$ is defined in the same way as k_v except that the optical potential U replaces the bound

state potential U_v .

Strictly Eq. (57) and Eq. (59) for δG and $\delta \bar{V}$ should contain some spin dependence. This comes from coupling between the valence nucleons and abnormal parity core excitations³⁵ and has been neglected primarily as a matter of convenience. It turns out that these spin dependent terms do not contribute to transitions between states of a (j^2) configuration as is shown in the Appendix. They do make a small contribution to the pairing energy, but we intend to compare Eq. (57) with appropriate two-body matrix elements rather than the experimental two-body spectra so their neglect causes no problem.

As examples, we consider the nuclei ^{50}Ti and ^{90}Zr both of which have two valence protons. The results of the lowest order microscopic calculations^{8,36} for the low-lying spectra of these nuclei are compared with experiment in Fig. 1. Results obtained with $(G + \delta G)$ and without (G) the inclusion of core polarization are both shown. In the calculation for ^{50}Ti a full f - p shell model space has been assumed for the two valence protons.⁸ The resulting wave functions for the lowest 0^+ , 2^+ , 4^+ , and 6^+ states are, however, almost pure $(1f_{7/2}^2)$ wave functions. In the calculation for ^{90}Zr the model space for the two valence protons included both the $(1g_{9/2}^2)$ and $(2p_{1/2}^2)$ configurations.³⁶ This explains the appearance of two 0^+ states in results for this nucleus.

The theoretical results with core polarization $(G + \delta G)$ are in good agreement with experiment in both cases. The pairing effect is quite evident. The multipole decomposition of the pairing matrix elements appearing in these calculations has been given in Refs. 8 and 36. Using Eq. (57) we obtain the following results for the pairing energy,

$$E_p(j) = \langle (j^2) 0^+ | \delta G | (j^2) 0^+ \rangle \\ = \sum_J E_p^J(j) \quad (60)$$

$$E_p^J(j) = -\langle k_v \rangle^2 \langle j || Y_J || j \rangle^2 \theta_J,$$

where $\langle k_v \rangle$ denotes the radial expectation of $k_v(r)$ and the sum on J runs over even values only. Assuming $\langle k_v \rangle \approx 50$ MeV and comparing Eq. (60) with the matrix elements of Refs. 8 and 36, we obtain the values of θ_J and C_J listed in Table I. From the table, we see that the core of ^{50}Ti is somewhat softer than that of ^{90}Zr and that $J=2$ core excitations give the dominant contribution to the pairing energy in both cases. The values of θ_J decrease steadily with increasing multipolarity; however, the core coupling is by no means negligible even for the highest core multipoles.

With the values of θ_J determined above, it is straightforward to estimate the corresponding

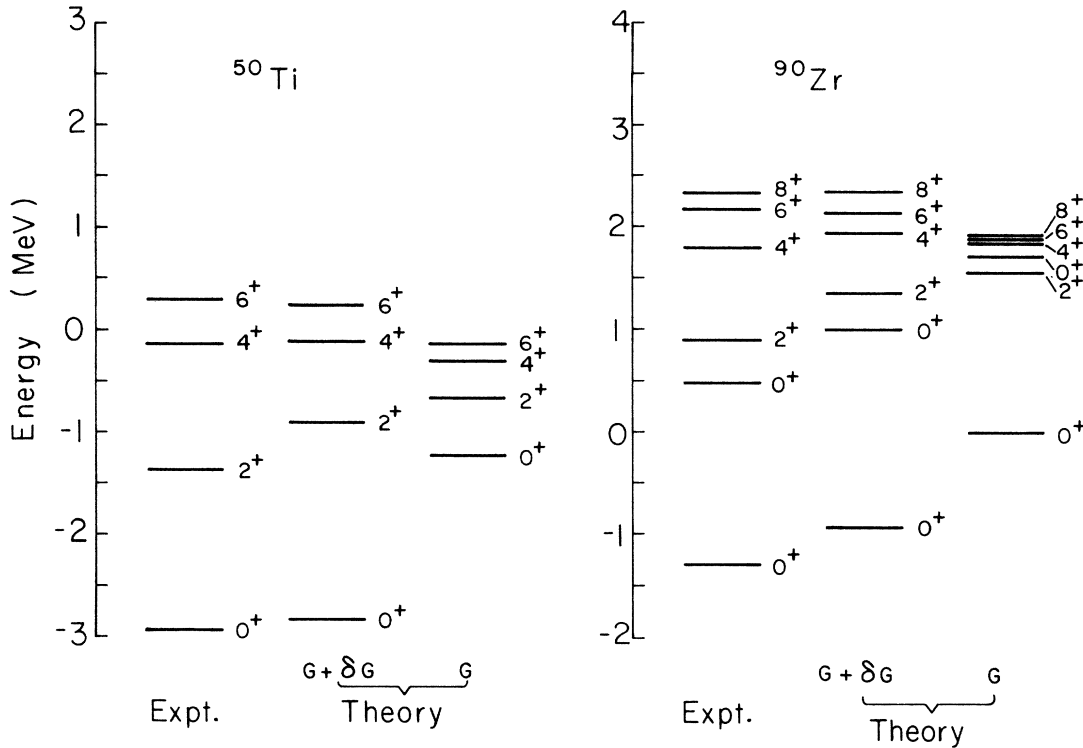


FIG. 1. Spectra of ^{50}Ti and ^{90}Zr showing pairing effect due to core polarization.

effect of core polarization in inelastic proton scattering. One simply constructs the valence radial form factor according to the prescription of Sec. IIA and adds to it the core correction

$$\delta \bar{F}^{LSJ}(r_p) = -\delta_{LJ} \delta_{\mathcal{S}0} (2/\hat{J}) \langle j \| Y_J \| j \rangle \langle k_v \rangle \theta_J k(r_p) \quad (61)$$

which follows directly from Eq. (59). Cross sections have been calculated for the excitation of the 2^+ and 4^+ levels in ^{50}Ti and the 2^+ , 4^+ , 6^+ , and 8^+ states in ^{90}Zr in this manner. The ^{50}Ti calculations were made for incident proton energies of 17.5 and 40 MeV to allow comparison with the experimental data of Refs. 37 and 38. The ^{90}Zr calculations were made for an incident proton energy of 18.8 MeV for comparison with the experimental data of Ref. 39. The optical parameters used in the calculations are tabulated in Table XII. The results are compared with the data in Figs. 2 and 3. The quantity ϵ_p^{LSJ} shown with each cross section is the enhancement factor for core polarization. This is defined by

$$\sigma^{LSJ} = (\epsilon_p^{LSJ})^2 \sigma_v^{LSJ}, \quad (62)$$

where σ and σ_v are the theoretical integrated cross sections with and without the inclusion of core polarization. The introduction of this enhancement factor is analogous to the use of effective charges

in describing electric γ transitions.

The theoretical results shown in Figs. 2 and 3 are in good qualitative agreement with experiment with the possible exception of the result for the 8^+ excitation in ^{90}Zr . It is suspected that multiple excitation might be important for this transition at this energy.¹⁸ We also note from the values of ϵ_p that core polarization leads to an increase in the valence cross section by at least an order of

TABLE I. Core coupling constants determined from bound state pairing matrix elements.

Nuclide	j	J	$E_p^J(j)^a$ (MeV)	θ_J (MeV ⁻¹)	C_J (MeV)
^{50}Ti	$1f_{7/2}$	0	-0.033	1.78×10^{-4}	5610
	$1f_{7/2}$	2	-0.753	3.18×10^{-3}	314
	$1f_{7/2}$	4	-0.460	2.20×10^{-3}	455
	$1f_{7/2}$	6	-0.233	1.55×10^{-3}	645
^{90}Zr	$1g_{9/2}$	0	-0.020	1.01×10^{-4}	9920
	$1g_{9/2}$	2	-0.578	2.38×10^{-3}	420
	$1g_{9/2}$	4	-0.359	1.58×10^{-3}	633
	$1g_{9/2}$	6	-0.218	1.14×10^{-3}	877
	$1g_{9/2}$	8	-0.122	9.00×10^{-4}	1110
	$2p_{1/2}$	0	-0.210	1.22×10^{-3}	820

^a Values for ^{50}Ti are from Ref. 8 and values for ^{90}Zr are from Ref. 36.

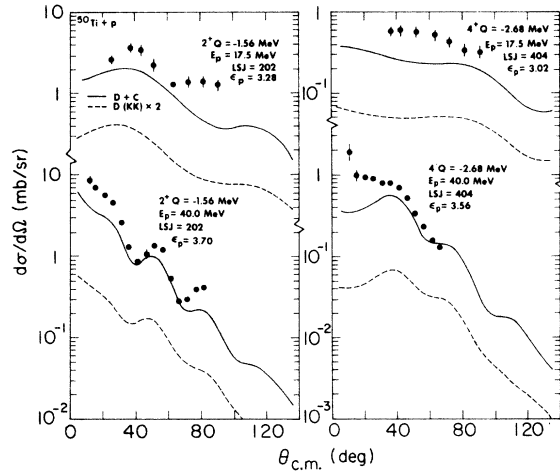


FIG. 2. Theoretical (p, p') differential cross sections obtained with schematic model for the first 2^+ and 4^+ states in ^{50}Ti with $E_p = 17.5$ and 40.0 MeV. Results with (D) and without $(D+C)$ core polarization are shown.

magnitude in each case. We conclude that there is a striking consistency in the effect of core polarization on the low-lying energy spectra of these nuclei and on the (p, p') cross sections for the excitation of these low-lying states.

The above results were previously reported elsewhere,⁴⁰ in less detail than given here, by two of the present authors. The parameters for ^{50}Ti from Table I were subsequently used in the calculation of theoretical (p, p') cross sections for low-lying excitations in ^{51}V .³⁸ This nucleus has three valence protons and the dominant configuration for the low-lying states is $(1f_{7/2})^3$. The theoretical results were found to be in good agreement

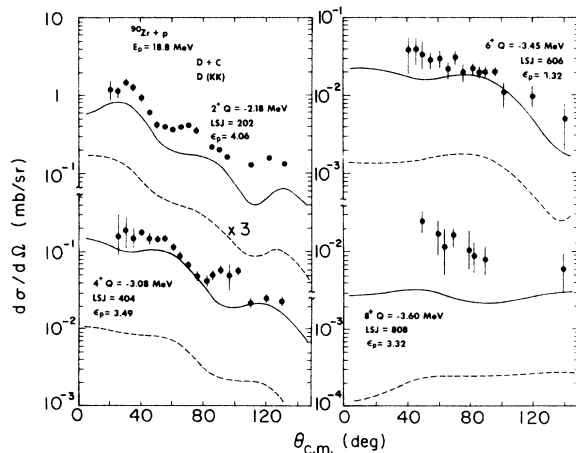


FIG. 3. Theoretical (p, p') differential cross sections obtained with schematic model for first 2^+ , 4^+ , 6^+ , and 8^+ states in ^{90}Zr with $E_p = 18.8$ MeV.

with experiment which tends to indicate that the effects of core polarization can be factorized, as lowest order perturbation theory implies, at least when the number of valence nucleons is small. A more recent (e, e') study of ^{51}V has provided evidence which contradicts this conclusion to some degree.⁴¹

To improve on first order estimates of $\delta\mathcal{T}$ it is necessary to include the effect of configuration interaction in the excluded space, which requires higher order perturbation theory. Formally these effects can be seen by rewriting Eqs. (39), (43), and (52) in the explicit representation:

$$\bar{G} = G + G \frac{Q}{E - H_0 - G} G, \quad (63)$$

$$N^2 = 1 + G \frac{Q}{(E - H_0 - G)^2} G, \quad (64)$$

$$\begin{aligned} \bar{\mathcal{T}} = & \mathcal{T} + \mathcal{T} \frac{Q}{E - H_0 - G} G + G \frac{Q}{E - H_0 - G} \mathcal{T} \\ & + G \frac{Q}{E - H_0 - G} \mathcal{T} \frac{Q}{E - H_0 - G} G. \end{aligned} \quad (65)$$

These relations are similar in structure to the lowest order perturbative expressions in that the coupling between the model space and the excluded space is given by G interactions alone [\bar{G} interactions appear on the right hand side in Eqs. (39), (43), and (52)]; however, the propagators in Eqs. (63)–(65) project onto eigenstates of H in the excluded space instead of eigenstates of H_0 as is true in the case of the lowest order perturbative expressions. The spectrum of H differs from that of H_0 due to the effect of G interactions in the excluded space and this in turn affects the results for \bar{G} , N^2 , and $\bar{\mathcal{T}}$.

Equations (63)–(65) cannot be evaluated exactly because it is impossible to diagonalize H in the excluded space which is still infinite; however, it is possible to evaluate these relations approximately by making suitable truncations in the excluded space. The effects of configuration interaction in the space of p - h excitations of the core is well established from the Tamm-Dancoff approximation (TDA) and random-phase approximation (RPA) calculations of Gillet and collaborators,⁴² i.e., it gives rise to low-lying normal parity vibrational states which are nearly isoscalar in character and pushes the isovector core excitations up in energy. Transitions provide many clear examples that these, or related and possibly more complicated, effects are important. For example, it has already been mentioned that experiment indicates that valence neutrons and protons have approximately equal polarization charges. This implies that the dominant coupling occurs with isoscalar

core excitations. Results obtained for inelastic proton scattering and γ transitions using the hydrodynamical core model^{15,43-46} provide another example of this same effect. Here, at least for transitions of low multipolarity, the coupling constants θ_J deduced from fits to inelastic proton scattering cross sections using Eq. (59) are found to be nearly equal to those required to reproduce the effective charge,¹⁵ i.e.,

$$e_{\text{eff}}^{Jq} = e_q + \theta_J \frac{3Z_c}{4\pi} eR_c^J \langle k_v \rangle / \langle r^J \rangle, \quad (66)$$

where $e_q = 1$ or 0 for $q = p$ or n , Z_c is the core charge, R_c its radius, and the radial expectations $\langle \rangle$ are taken with respect to the radial wave functions of the valence nucleons. The θ_J in Eq. (59) and Eq. (66) are only equal in the limit of coupling to isoscalar core excitations.³⁵ [Note that our schematic discussion of the relationship between the pairing effect and the enhancement of (p, p') cross sections required no reference to the isospin nature of the coupling between the core and the valence protons.] A third and perhaps even more striking example of the importance of configuration interaction in the excluded space is seen in nuclei around ²⁰⁸Pb where there are clear-cut cases of coupling between valence nucleons and low-lying vibrational states of the core.^{43,17}

Including only the effect of configuration interaction in the core by means of the TDA or RPA approximations seems to provide the best estimate of transition matrix elements insofar as agreement with experiment is concerned.¹⁰ These calculations are equivalent to assuming a particle-vibrational model and preserve the factorizability of core polarization effects. Similar calculations for \bar{G} result in an overestimation of the pairing energy.^{9,11} One would like to find a suitable approximation for evaluating Eqs. (63)–(65) which would improve the lowest order estimates of the transition matrix elements and at the same time preserve the lowest order results of Kuo and Brown for the effective interaction. So far this has not been accomplished.¹¹ In fact, the most complete treatment of the effect of configuration interaction in the excluded space which has been made to date¹¹ leads to results for \bar{G} which are not much different than those for G and results for $\bar{\mathcal{T}}$ which are similar to those obtained using first order perturbation theory.

Harvey and Khanna have suggested³⁴ that a possible way of bootstrapping the effect on $\bar{\mathcal{T}}$ of configuration interaction in the excluded space might be to use Eq. (43) and Eq. (52) approximating \bar{G} by a two-body interaction \bar{G}' which fits the two-body spectra. They point out that this procedure was fol-

lowed by Horie and Arima² in their early calculations. Owing to the uncertainty in the perturbative treatment of these higher order effects¹¹ and faced with the need of including some estimate of the effect of core correlations, we have crudely followed this approach for our second estimate of the matrix elements of $\bar{\mathcal{T}}$. Specifically, we have repeated the first order calculations using the renormalized core coupling interaction

$$\bar{G}' = G - \sum_{\substack{i < j \\ J_M}} \theta_J k_v(r_i) k_v(r_j) Y_{J_M}^*(\hat{r}_i) Y_{J_M}(\hat{r}_j) P_1^{\mathcal{T}}, \quad (67)$$

where $P_1^{\mathcal{T}}$ projects onto triplet isospin states and the θ_J are fixed from the pairing matrix elements of Refs. 8 and 36 in the manner described above. This interaction is somewhat incomplete in that it does not contain any spin dependence and is missing some small renormalization terms which act in isospin singlet states. It does, however, contain the major components required to fit the two-body spectra. In Sec. IV, it will be seen that the results obtained using this interaction are similar to those obtained using the "bare" G and treating core correlations in the TDA approximation.^{10,11}

C. Explicit expressions for matrix elements of $\bar{\mathcal{T}}$

In this section we construct the explicit expression for the reduced matrix element of $\bar{\mathcal{T}}$ between two model space states. This is obtained directly from the expressions for the amplitudes of the excluded space configurations in the model space configurations and the reduced matrix elements for \mathcal{T} between two model space states and between a model space state and an excluded space state. We consider only one-body operators which transform like the spin-angle tensor defined in Eq. (17) and throughout this section the use of G is intended to imply either G or \bar{G}' .

We define the model space states by

$$|\phi_{\mathbf{M}}\rangle = |\alpha_1(n)J_1M_1\rangle = Z_{\alpha_1 J_1 M_1}^\dagger(n)|C\rangle, \quad (68)$$

where $Z_{\alpha_1 J_1 M_1}^\dagger(n)$ creates an np or nh state with quantum numbers α_1, J_1, M_1 by operating on the closed shell state $|C\rangle$. J_1 and M_1 denote the total angular momentum and projection while α_1 represents all other quantum numbers required to completely specify the state.

In first order only $(n+1)p-1h[(n+1)h-1p]$ and $np(nh)$ intermediate states can contribute to the renormalization of \mathcal{T} . We include only the former with the remark that the latter are best included in the model space whenever they are important. The $(n+1)p-1h[(n+1)h-1p]$ excluded space states are defined by

$$\begin{aligned}
|\phi_E\rangle &= |\alpha_2(n)J_2, (\overline{p\bar{h}})J_c; J_3 M_3\rangle \\
&= \sum_{M_2 M_c} \langle J_2 J_c M_2 M_c | J_3 M_3 \rangle Z_{\alpha_2 J_2 M_2}^\dagger(n) A_{J_c M_c}^\dagger(\text{ph}) |C\rangle,
\end{aligned} \tag{69}$$

where

$$A_{J_c M_c}^\dagger(\text{ph}) = \sum_{m_p m_h} \langle j_p j_h m_p -m_h | J_c M_c \rangle (-1)^{j_h - m_h} a_p^\dagger a_h \tag{70}$$

creates a p-h pair with angular momentum J_c and projection M_c . In writing Eq. (69) it has been assumed that p and h are distinct from any of the particle or hole states contained in $Z_{\alpha_2 J_2 M_2}^\dagger(n)$, i. e., we neglect the Pauli principle in intermediate states. The error introduced by making this simplification should not be serious because we consider only cases where n is relatively small.

The amplitude of the excluded space with energy $\epsilon_{\alpha_2 J_2 \text{ph}}$ in the model space state with energy $\epsilon_{\alpha_1 J_1}$ is easily found to be

$$a(\alpha_2 J_2, (\overline{p\bar{h}})J_c; J_3 | \alpha_1 J_1) = \delta_{J_1 J_3} (-1)^{J_2 - J_1} \hat{j}_p \hat{j}_2 \hat{j}_1^{-1} \sum_{J_c' \gamma} S_q^{J_c'}(\alpha_2 J_2, \alpha_1 J_1; j_\alpha j_\gamma) \alpha_{q_0}^{J_c'}(j_p j_h, j_\alpha j_\gamma) / (\epsilon_{\alpha_1 J_1} - \epsilon_{\alpha_2 J_2 \text{ph}}), \tag{71}$$

where

$$S_q^{J_c}(\alpha_2 J_2, \alpha_1 J_1; j_\alpha j_\gamma) = \hat{j}_\alpha \hat{j}_c^{-1} \langle \alpha_2(n)J_2 || A_{J_c}^\dagger(\alpha\gamma) || \alpha_1(n)J_1 \rangle \tag{72}$$

is a spectroscopic amplitude which depends only on the structure of the valence configurations, and

$$\alpha_{q_0}^{J_c'}(j_p j_h, j_\alpha j_\gamma) = \sum_{J'} (-1)^{j_\alpha + j_h - J'} \frac{\hat{j}_c \hat{j}_2}{\hat{j}_p \hat{j}_\alpha} \begin{Bmatrix} j_p & j_\alpha & J' \\ j_\gamma & j_h & J_c \end{Bmatrix} \langle j_p j_\alpha J' | g_{qq'} | j_h j_\gamma J' \rangle_a \tag{73}$$

is the J th multipole coefficient of the coupling interaction. The indices q and q' which appear in Eq. (72) and (73) specify the charge state of the valence particles ($j_\alpha j_\gamma$) and the core excitation ($j_p j_h$), respectively. This in turn determines which component of g is effective in the polarizing process. The subscript a on the two-body matrix element in Eq. (73) indicates that the matrix element is antisymmetrized but not normalized. The values of $S_q^{J_c}$ for the transitions of interest in this work are given in the Appendix. It is the separation of the amplitude of Eq. (66) into a geometrical factor $S_q^{J_c}$ and a dynamical factor $\alpha_{q_0}^{J_c}$, which gives rise to the factorizability of core polarization effects in lowest order. Additional factorization of $\alpha_{q_0}^{J_c}$ into valence and core parts is the essential feature built into all phenomenological models for effective operators.^{15,35,47,48}

We also note the following symmetry relations for $S_q^{J_c}$ and $\alpha_{q_0}^{J_c}$:

$$\begin{aligned}
S_q^{J_c}(\alpha_1 J_1, \alpha_2 J_2; j_\alpha j_\gamma) &= (-1)^{J_1 - J_2 + j_\gamma - j_\alpha} \hat{j}_2 \hat{j}_\alpha \hat{j}_1^{-1} \hat{j}_\gamma^{-1} \\
&\quad \times S_q^{J_c}(\alpha_2 J_2, \alpha_1 J_1; j_\gamma j_\alpha), \tag{74}
\end{aligned}$$

$$\begin{aligned}
\alpha_{q_0}^{J_c'}(j_p j_h, j_\alpha j_\gamma) &= (-1)^{j_\alpha - j_\gamma + j_h - j_p} \hat{j}_h \hat{j}_\gamma \hat{j}_\alpha^{-1} \hat{j}_p^{-1} \\
&\quad \times \alpha_{q_0}^{J_c'}(j_h j_p, j_\gamma j_\alpha). \tag{75}
\end{aligned}$$

As an example of the usefulness of these relations, we observe that they may be used to show that

$$\begin{aligned}
a(\alpha_2 J_2 (\overline{p\bar{h}})J_c; J_1 | \alpha_1 J_1) \\
= (-1)^{J_2 - J_1} \hat{j}_2 \hat{j}_1^{-1} a(\alpha_1 J_1, (\overline{p\bar{h}})J_c; J_2 | \alpha_2 J_2)
\end{aligned} \tag{76}$$

in cases when there is only one active orbit in the states $\alpha_1 J_1$ and $\alpha_2 J_2$, i. e., $j_\alpha = j_\gamma = j$.

The reduced matrix element of a one-body operator \mathcal{T}^{LSJ} taken between a model space and an excluded space state is

$$\langle \phi_E || \mathcal{T}^{LSJ} || \phi_M \rangle = \delta_{\alpha_1 \alpha_2} \delta_{J_1 J_2} \delta_{J_c} \hat{j}_p \hat{j}_\alpha^{-1} \langle j_p || t_q^{LSJ} || j_h \rangle, \tag{77}$$

where the superscripts LSJ have been added to \mathcal{T} since we consider operators which transform like the spin-angle tensor of Eq. (17). The subscript q appearing on t_q^{LSJ} in this equation is a charge index. It is needed because, in general, t_q^{LSJ} will not be the same for a proton p-h pair and a neutron p-h pair. The main point to notice about the result is that the p-h pair is produced solely by the action of \mathcal{T} , with the valence nucleons serving merely as spectators. The result for the reversed matrix element $\langle \phi_M || \mathcal{T}^{LSJ} || \phi_E \rangle$ will not be given since it easily derived from the following conjugation relation for operators of the spin-angle type:

$$\langle J_a || T^{LSJ} || J_b \rangle = (-1)^{S+J+J_a-J_b} \hat{j}_b \hat{j}_a^{-1} \langle J_b || T^{LSJ} || J_a \rangle. \tag{78}$$

The reduced matrix element of \mathcal{T}^{LSJ} between two model space states is simply

$$\begin{aligned}
\langle \alpha_2(n)J_2 || \mathcal{T}^{LSJ} || \alpha_1(n)J_1 \rangle \\
= \sum_{J_c' \gamma} S_q^{J_c'}(\alpha_2 J_2, \alpha_1 J_1; j_\alpha j_\gamma) \langle j_\alpha || t_q^{LSJ} || j_\gamma \rangle.
\end{aligned} \tag{79}$$

Use of the above results for the matrix elements of \mathcal{T} and G and the associated symmetry and conjugation relations in Eq. (56) leads directly to the expression for the reduced matrix element of the

$$\langle \alpha_f(n)J_f \| \bar{\mathcal{T}}^{LSJ} \| \alpha_i(n)J_i \rangle = \sum_{j_\alpha j_\gamma} S_q^J(\alpha_f J_f, \alpha_i J_i; j_\alpha j_\gamma) \left[\langle j_\alpha \| t_q^{LSJ} \| j_\gamma \rangle + \sum_{j_p j_h} \left(\frac{1}{\epsilon_{\alpha_i J_i} - \epsilon_{\alpha_f J_f \text{ph}}} + \frac{1}{\epsilon_{\alpha_f J_f} - \epsilon_{\alpha_i J_i \text{ph}}} P_{\text{ph}} \right) F_{q\alpha'}^J(j_p j_h, j_\alpha j_\gamma) \right], \quad (80)$$

where P_{ph} acts to the right and means to interchange j_p and j_h , and

$$F_{q\alpha'}^J(j_p j_h, j_\alpha j_\gamma) = (-1)^{j_p - j_h} \hat{j}_p \hat{j}_h \hat{j}^{-1} \alpha_{q\alpha'}^J(j_p j_h, j_\alpha j_\gamma) \langle j_h \| t_q^{LSJ} \| j_p \rangle. \quad (81)$$

In Eq. (80) the first term on the left is the normal valence contribution and the second term is the core polarization contribution. Using Eq. (75) and Eq. (78) in Eq. (81) we also note that

$$P_{\text{ph}} F_{q\alpha'}^J(j_p j_h, j_\alpha j_\gamma) = (-1)^{S+J-j_\alpha-j_\gamma} \hat{j}_\alpha \hat{j}_\gamma^{-1} F_{q\alpha'}^J(j_p j_h, j_\gamma j_\alpha). \quad (82)$$

D. Enhancement and retardation of transition operators

The expression for the reduced matrix element $\bar{\mathcal{T}}$ given in the preceding section can be reduced further by specializing to the case of a zero-range coupling interaction, i.e.,

$$g_{q\alpha'}(1, 2) = (g_{q\alpha'}^0 + g_{q\alpha'}^1 \hat{\sigma}_1 \cdot \hat{\sigma}_2) \delta(\vec{r}_1 - \vec{r}_2). \quad (83)$$

We pursue this here as it allows us to derive a general rule concerning the phase of the contribution from core polarization. Calculations using typical finite-range interactions produce results consistent with this rule.

The derivation requires further specification of the form of the one-body operator of interest. We consider only one-body operators which can be written

$$t_q^J = f_q^{LSJ} T^{LSJ} = \beta_q^{LSJ} h_q^{LSJ} T^{LSJ}, \quad (84)$$

where T^{LSJ} is the spin-angle tensor defined in Eq. (17) and f_q^{LSJ} contains the radial dependence

$$\langle \alpha_f(n)J_f \| \bar{\mathcal{T}}^{LSJ} \| \alpha_i(n)J_i \rangle = \sum_{j_\alpha j_\gamma} S_q^J(\alpha_f J_f, \alpha_i J_i; j_\alpha j_\gamma) \left[\langle j_\alpha \| T^{LSJ} \| j_\gamma \rangle \langle h_q^{LSJ} \rangle_{\alpha\gamma} \beta_q^{LSJ} + \sum_{L'S'} \langle j_\alpha \| T^{L'S'} \| j_\gamma \rangle H_{L'S'}^{LSJ}(\alpha, \gamma) \right], \quad (88)$$

where

$$H_{L'S'}^{LSJ}(\alpha, \gamma) = - \sum_{j_p j_h} \frac{\epsilon(\text{ph})}{\epsilon^2(\text{ph}) - Q^2} \frac{4\hat{j}_p^2}{\hat{j}^2} g_{q\alpha'}^S \langle j_p \| T^{LSJ} \| j_h \rangle \langle j_p \| T^{L'S'} \| j_h \rangle I(l_p l_\alpha l_h l_\gamma) \langle h_q^{LSJ} \rangle_{\text{ph}} \beta_q^{LSJ} \quad (89)$$

and

renormalized transition operator taken between two model space states. This is the essential relation for the calculations of this work. The result is

of the operator, h_q^{LSJ} , as well as the coupling constant, β_q^{LSJ} , e.g., $h_q^{LSJ} = \delta_{S0} \delta_{LJ} r^L$ and $\beta_q^{LSJ} = e_q$ in the case of an electric γ transition.

In the case of a zero-range interaction the direct and exchange parts of two-body matrix elements are identical and the multipole coefficient of Eq. (73) can be factorized, i.e.,

$$\alpha_{q\alpha'}^J(j_p j_h, j_\alpha j_\gamma) = \frac{2}{\hat{j}} \sum_{L'S} g_{q\alpha'}^S (-1)^{S+J} \langle j_p \| T^{LSJ} \| j_h \rangle \times \langle j_\alpha \| T^{LSJ} \| j_\gamma \rangle I(l_p l_h l_\alpha l_\gamma). \quad (85)$$

The reduced matrix elements in Eq. (85) contain only integrations over spin and angular coordinates and I is a radial overlap integral

$$I(l_p l_h l_\alpha l_\gamma) = \int_0^\infty u_p(r) u_\alpha(r) u_h(r) u_\gamma(r) r^2 dr, \quad (86)$$

where the $u(r)$ denote single particle radial wave functions. The factorization of $\alpha_{q\alpha'}^J$ further implies that

$$P_{\text{ph}} F_{q\alpha'}^J(j_p j_h, j_\alpha j_\gamma) = F_{q\alpha'}^J(j_p j_h, j_\alpha j_\gamma) \quad (87)$$

which is easily demonstrated using Eq. (78) and Eq. (85) in Eq. (82). Using Eq. (84), (85), and (86) in Eq. (80) we obtain the desired result for the matrix element of $\bar{\mathcal{T}}$ in the case of a zero-range coupling interaction. This is

$$\langle h_q^{LSJ} \rangle_{\text{ph}} = \int_0^\infty u_p(r) h_q^{LSJ} u_h(r) r^2 dr, \quad (90)$$

$$\epsilon(\text{ph}) = \epsilon_p - \epsilon_h, \quad Q = \epsilon_{\alpha_i j_i} - \epsilon_{\alpha_f j_f}. \quad (91)$$

The phase rule of interest applies only to a single pair of active valence orbitals, i.e., fixed $j_\alpha j_\gamma q$. The phase relation between different terms in the sum over $j_\alpha j_\gamma q$ is a function of the model space configurations and not of core polarization. Restricting consideration to a fixed set of values for $j_\alpha j_\gamma q$ we have only to consider the sum over L' and S' in Eq. (88). Owing to parity and angular momentum selection rules, there are only two allowed sets of values of $L'S'$ for given LSJ . It is sufficient to note that one set is $L'S' = LS$ and the other is $L'S' \neq LS$.

For the first set, $L'S' = LS$, we note that the sign of each term in the sum over j_p and j_h in Eq. (89) is given by

$$- \sum_{q'} g_{qq'}^S \langle h_q^{LSJ} \rangle_{\text{ph}} I(l_p l_\alpha l_h l_\gamma) \beta_q^{LSJ},$$

where it has been assumed that $\epsilon^2(\text{ph}) > Q^2$. We then argue that the important terms in the sum over j_p and j_h are those where

$$u_p(r) u_h(r) \approx u_\alpha(r) u_\gamma(r).$$

This is sufficient to guarantee that for these important terms

$$I(l_p l_\alpha l_h l_\gamma) > 0, \\ \langle h_q^{LSJ} \rangle_{\text{ph}} \approx \langle h_q^{LSJ} \rangle_{\alpha\gamma}.$$

Considering only the contribution from the term H_{LS}^{LSJ} to the renormalization of the matrix element of \mathcal{T}^{LSJ} , we conclude that the relative signs of the valence and core contribution are given by

$$\langle \mathcal{T}^{LSJ} \rangle_{fi} \sim \beta_q^{LSJ} \quad (92) \\ \langle \delta \mathcal{T}^{LSJ} \rangle_{fi} \sim - \sum_{q'} \beta_q^{LSJ} g_{qq'}^S.$$

$$\delta t_q^{L'S'J}(\mathbf{r}_i) = - \sum_{j_p j_h} \frac{\epsilon(\text{ph})}{\epsilon^2(\text{ph}) - Q^2} \frac{4\hat{j}_p^2}{\hat{j}^2} \langle j_p \| T^{LSJ} \| j_h \rangle \langle j_p \| T^{L'S'J} \| j_h \rangle g_{qq'}^{S'} \beta_q^{LSJ} \langle h_q^{LSJ} \rangle_{\text{ph}} u_p(r_i) u_h(r_i). \quad (94)$$

An operator of this form has been used to fit the magnetic moments in the Pb region.⁴⁸ The force strengths $g_{qq'}^S$ were treated as adjustable parameters in obtaining the fit. This approach could be extended to other one-body operators.

IV. RESULTS

In this section we present the results of our calculations for selected transitions in ⁴²Ca, ⁵⁰Ti, ⁸⁹Y, ⁹⁰Zr, ²⁰⁷Pb, and ²⁰⁹Bi. The nuclides ⁵⁰Ti and

Finally we argue that the contribution from the term $H_{L'S'}^{L'S'J}$ with $L'S' \neq LS$ can, in fact, be neglected, because the various terms comprising this quantity have random phases.

Using Eq. (92) it is a simple matter to compute the relative sign of the valence contribution and the core polarization contribution for a given one-body operator. For inelastic proton scattering we have $\beta_q^{LSJ} = \bar{V}_{pq}^S$ from Eq. (14). Using the fact that $\bar{V}_{pq}^S \sim g_{pq}^S$ and the relationship between the components of g_{pq}^S given in Eq. (4), it immediately follows that the valence and core contribution are in phase for $S=0$ amplitudes and out of phase for $S=1$ amplitudes, i.e., the $S=0$ amplitudes are enhanced while the $S=1$ amplitudes are retarded.

For longitudinal electron scattering and electric γ transitions $S=0$ and $\beta_q^{LSJ} = e_\gamma = 0$ or 1 , as $q=p$ or n . Since g_{pq}^0 is attractive, we conclude that the valence and core contributions are in phase for this case. For magnetic γ transitions $S=1$ and $\beta_q^{LSJ} = \mu_q$ which is positive or negative as $q=p$ or n . Using Eq. (4) we find that the valence and core contributions are out of phase. These results demonstrate that there is a close correspondence between the effects of core polarization in inelastic proton scattering and in electromagnetic interactions.

It is possible to go one step beyond Eqs. (88)–(91) and write a closed coordinate space expression for $\delta \mathcal{T}^J$. This is

$$\delta \mathcal{T}_{M_J}^{L'S'J} = \sum_i \delta t_q^{L'S'J}(\mathbf{r}_i) T_{M_J}^{L'S'J}(\mathbf{i}), \quad (93)$$

where the sum on i runs only over the valence nucleons and $q=p$ or n , as i designates a proton or a neutron. The radial factors in Eq. (93) are given by

⁹⁰Zr have already been discussed in connection with the schematic model in Sec. III B. They have two valence protons outside of ⁴⁸Ca and ⁸⁸Sr cores, respectively. ⁴²Ca has two valence neutrons outside a ⁴⁰Ca core; ⁸⁹Y has one valence proton outside a ⁸⁸Sr core; ²⁰⁷Pb has one valence neutron hole in a ²⁰⁸Pb core; while ²⁰⁹Bi has a single valence proton outside a ²⁰⁸Pb core. The transitions we have considered are summarized in Table II. The initial and final model space wave function assumed in each case are specified in the table.

TABLE II. Summary of transitions considered in this work. Initial and final model space wave functions are given in each case.

Target ^a	J_i^{π}	$ \phi_M^i\rangle$	J_f^{π}	$ \phi_M^f\rangle$	Q^b (MeV)
⁴² Ca(2n)	0 ⁺	$ (1f_{7/2}^2)0\rangle$	2 ⁺	$ (1f_{7/2}^2)2\rangle$	-1.52
			4 ⁺	$ (1f_{7/2}^2)4\rangle$	-2.76
			6 ⁺	$ (1f_{7/2}^2)6\rangle$	-3.19
⁵⁰ Ti(2p)	0 ⁺	$ (1f_{7/2}^2)0\rangle$	2 ⁺	$ (1f_{7/2}^2)2\rangle$	-1.56
			4 ⁺	$ (1f_{7/2}^2)4\rangle$	-2.68
			6 ⁺	$ (1f_{7/2}^2)6\rangle$	-3.20
⁸⁹ Y(1p)	$\frac{1}{2}^-$	$ 2p_{1/2}\rangle$	$\frac{9}{2}^+$	$ 1g_{9/2}\rangle$	-0.91
⁹⁰ Zr(2p)	0 ⁺	$0.8 (2p_{1/2}^2)0\rangle$ $+ 0.6 (1g_{9/2}^2)0\rangle$	2 ⁺	$ (1g_{9/2}^2)2\rangle$	-2.18
			4 ⁺	$ (1g_{9/2}^2)4\rangle$	-3.08
			6 ⁺	$ (1g_{9/2}^2)6\rangle$	-3.45
			8 ⁺	$ (1g_{9/2}^2)8\rangle$	-3.60
²⁰⁷ Pb(1n ⁻¹)	$\frac{1}{2}^-$	$ 3p_{1/2}^{-1}\rangle$	5 ⁻	$ 2f_{5/2}^{-1}\rangle$	-0.57
			$\frac{3}{2}^-$	$ 3p_{3/2}^{-1}\rangle$	-0.89
			$\frac{1}{2}^-$	$ 1i_{13/2}^{-1}\rangle$	-1.63
			$\frac{3}{2}^-$	$ 2f_{7/2}^{-1}\rangle$	-2.33
			$\frac{1}{2}^-$	$ 2f_{7/2}^{-1}\rangle$	-2.33
²⁰⁹ Bi(1p)	$\frac{9}{2}^+$	$ 1h_{9/2}\rangle$	$\frac{7}{2}^-$	$ 2f_{7/2}\rangle$	-0.90
			$\frac{13}{2}^+$	$ 1i_{13/2}\rangle$	-1.61

^aThe number and type of valence nucleons is indicated in parentheses.

^bThis column lists experimental Q value which is not to be confused with theoretical Q value defined in Eq. (91).

A. Parameters of the calculations

For the first order estimates of $\delta\mathcal{T}$ we have used the long-range part of the Kallio-Kolltveit (KK) potential⁴⁹ for G . This is an S-wave interaction which gives matrix elements which are in rough agreement with those obtained with the more realistic HJ interaction.⁵ The S-wave form of the KK force greatly simplifies the calculation of two-body matrix elements. This feature has made this interaction popular in the past¹⁰ and it is also the main reason why it has been chosen here. The differences between the KK and HJ interaction are well within the accuracy of the models being used in this work, so there is no real inconsistency in using the KK force for G in calculating the bound state matrix elements and using the HJ interaction for $t_{i,p}^R$ in calculating the (p, p') cross sections.

For ⁵⁰Ti and ⁹⁰Zr, in the calculations of $\delta\mathcal{T}$ using the renormalized coupling interaction defined in Eq. (67), we have used the values of $\theta_L^P = 1/C_L^P$ given in Table I. The ⁹⁰Zr parameters were also used in the calculations for ⁸⁹Y. For ⁴²Ca we have used $C_0^P = 6020$ MeV, $C_2^P = 355$ MeV, $C_4^P = 578$ MeV, and $C_6^P = 1050$ MeV and in the Pb region we have used $C_0^P = 3790$ MeV, $C_2^P = 1040$ MeV, $C_4^P = 1580$ MeV, $C_6^P = 2450$ MeV, and $C_8^P = 3650$ MeV. These

last two sets of values have been determined from matrix elements given in Ref. 8 in the same manner that was used to determine the values given in Table I. It is interesting to note the large increase in the stiffness of the core in passing from the Ca region to the Pb region.

We do not actually evaluate the radial integrals $\langle k_v \rangle$ which arise in the calculation of the matrix elements of \bar{G}' . Instead we assume that

$$\langle k_v \rangle_{13} \langle k_v \rangle_{24} = 2500 f(n_1 n_3; n_2 n_4) \text{ MeV}^2,$$

where $n(=1, 2, \dots, \infty)$ denotes the principle quantum number which characterizes the shape of the radial wave functions. The factor

$$f(n_1 n_3; n_2 n_4) = (-1)^{|n_1 - n_3| + |n_2 - n_4|} (0.75)^{n_1 + n_2 + n_3 + n_4 - 4}$$

has the value unity when $n_1 = n_2 = n_3 = n_4 = 1$, i.e., when all of the radial wave functions have good overlap with $k_v(r)$, and is appropriately smaller and properly phased when there are shape differences between the radial wave functions and $k_v(r)$.

Harmonic oscillator radial wave functions have been used throughout in the calculations. The oscillator well parameter $\alpha = (M\omega/\hbar)^{1/2} \text{ fm}^{-1}$ has been fixed according to³¹

$$\hbar\omega = 41A^{-1/3} \text{ MeV}.$$

TABLE III. Single particle energies for spherical potential as determined by Nilsson.

No.	N^a	nlj^{π}	$E_{nlj}/\hbar\omega^b$	No.	N^a	nlj^{π}	$E_{nlj}/\hbar\omega^b$
1	0	$1s_{1/2}^+$	1.50	21	5	$2f_{5/2}^-$	6.43
2	1	$1p_{3/2}^-$	2.45	22	5	$3p_{1/2}^-$	6.56
3	1	$1p_{1/2}^-$	2.60	23	6	$2g_{9/2}^+$	6.85
4	2	$1d_{5/2}^+$	3.40	24	6	$1i_{11/2}^+$	6.91
5	2	$2s_{1/2}^+$	3.50	25	7	$1j_{15/2}^+$	7.03
6	2	$1d_{3/2}^+$	3.65	26	6	$3d_{5/2}^+$	7.27
7	3	$1f_{7/2}^-$	4.14	27	6	$2g_{7/2}^+$	7.30
8	3	$2p_{3/2}^-$	4.42	28	6	$4s_{1/2}^+$	7.50
9	3	$1f_{5/2}^-$	4.49	29	6	$3d_{3/2}^+$	7.52
10	3	$2p_{1/2}^-$	4.57	30	7	$2h_{11/2}^-$	7.65
11	4	$1g_{9/2}^+$	4.85	31	8	$1k_{17/2}^+$	7.66
12	4	$2d_{5/2}^+$	5.27	32	7	$1j_{13/2}^-$	7.78
13	4	$1g_{7/2}^+$	5.30	33	7	$3f_{7/2}^-$	8.11
14	4	$3s_{1/2}^+$	5.50	34	7	$2h_{9/2}^-$	8.20
15	4	$2d_{3/2}^+$	5.52	35	9	$1i_{19/2}^-$	8.25
16	5	$1h_{11/2}^-$	5.58	36	8	$2i_{13/2}^+$	8.36
17	5	$2f_{7/2}^-$	6.08	37	7	$4p_{3/2}^-$	8.44
18	5	$1h_{9/2}^-$	6.13	38	7	$3f_{5/2}^-$	8.46
19	6	$1i_{13/2}^+$	6.26	39	8	$1k_{15/2}^+$	8.56
20	5	$3p_{3/2}^-$	6.41	40	7	$4p_{1/2}^-$	8.59

^a $N=2(n-1)+l$ is the major shell quantum number.

^b $E_{nlj}/\hbar\omega=N-0.05j(j+1)+0.05(1-\mu)l(l+1)+1.5375$

where $\hbar\omega$ determines the major shell separation:

$\mu=0.00$, $N=0, 1, 2$; $\mu=0.35$, $N=3$; $\mu=0.45$, $N=4, 5, 6$; and $\mu=0.40$, $N=7$.

The energy denominators used in the calculations were taken for the most part from the zero deformation axis of the Nilsson scheme.⁵⁰ In some cases they were taken from experiment. The Nilsson energies for the first 40 single particle states are given in Table III as a function of $\hbar\omega$. In the table each single particle state has been assigned an identification number as a matter of convenience.

The range of intermediate states used in esti-

mating $\delta\mathcal{T}$ for the various transitions being considered is summarized in Table IV. All possible $(n+1)p-1h$ [$(n+1)h-1p$] states which can be obtained by raising a core nucleon from one of the single particle states designated as a hole level to one of the single particle states designated as a particle level have been included in the calculations of $\delta\mathcal{T}$. Inspection of the table will show that we have "approximately" followed the rule of including all $(n+1)p-1h$ [$(n+1)h-1p$] intermediate states with energies up to $2\hbar\omega$ for positive parity transitions and $1\hbar\omega$ for negative parity transitions.

Experimental single particle energies have been used for the $1\hbar\omega$ positive parity core excitations which enter the calculations of $\delta\mathcal{T}$ for transitions in ⁵⁰Ti and ⁹⁰Zr. The energies of these particular core excitations are relatively small and the Nilsson scheme cannot be expected to be reliable in these cases. Specifically, we use experimental energy splittings for the $2p_{3/2}-1f_{7/2}^{-1}$, $2p_{1/2}-1f_{7/2}^{-1}$, and $1f_{5/2}-1f_{7/2}^{-1}$ neutron excitations in ⁵⁰Ti, the $2p_{1/2}-2p_{3/2}^{-1}$, $2p_{1/2}-1f_{5/2}^{-1}$, and $2p_{1/2}-1f_{7/2}^{-1}$ proton excitations in ⁹⁰Zr, and the $2d_{5/2}-1g_{9/2}^{-1}$, $3s_{1/2}-1g_{9/2}^{-1}$, $2d_{3/2}-1g_{9/2}^{-1}$, and $1g_{7/2}-1g_{9/2}^{-1}$ neutron excitations in ⁹⁰Zr. The experimental energy splittings are, respectively, 4.80, 6.82, and 8.75 MeV,⁸ 3.5, 4.0, and 5.5 MeV,^{51, 52} and 4.50, 5.53, 6.50, and 7.17 MeV^{51, 52} which are typically larger than the values which would be deduced from Table III. For the calculations in the Pb region we chose to use experimental energy values in all cases where they were available, namely, proton levels Nos. 11-22 and 24 and neutron levels Nos., 16-29 and 32.⁵³ The Nilsson energies were used for the other levels with some slight modifications. These were to increase the Nilsson energies for proton orbitals Nos. 23, 25, and above by 2.41 MeV, so that level No. 23 would not fall below level No. 24, and to make the neutron

TABLE IV. Particle and hole levels used to form intermediate states in the perturbative calculations of $\delta\mathcal{T}$.

Target	Transitions (J_f^{π})	Hole levels		Particle levels	
		Protons No.	Neutrons No.	Protons No.	Neutrons No.
⁴² Ca	$2^+, 4^+, 6^+$	2-6	2-6	7-15	7-15
⁵⁰ Ti	$2^+, 4^+, 6^+$	2-6	2-7	7-15	8-15
⁸⁹ Y	$\frac{3}{2}^+$	7-9	7-11	10-23	12-23
⁹⁰ Zr	$2^+, 4^+, 6^+, 8^+$	4-9	4-11	10-23	12-23
⁹⁰ Zr	5^-	7-9	7-11	10-23	12-23
²⁰⁷ Pb	$\frac{3}{2}^-, \frac{5}{2}^-, \frac{7}{2}^-$	7-16	11-22	17-35	23-35
²⁰⁷ Pb	$\frac{13}{2}^+$	11-16	16-22	17-30	23-34
²⁰⁹ Bi	$\frac{7}{2}^-$	7-16	11-22	17-35	23-35
²⁰⁹ Bi	$\frac{13}{2}^+$	11-16	16-22	17-30	23-34

levels Nos. 30 and 31 degenerate with level No. 32 instead of below it as the Nilsson scheme suggests.

B. Wave functions

It is useful to examine the most important core admixtures in the various model space configurations being treated. Owing to space limitations we consider only two typical examples here. More complete information can be obtained from the authors by request.

Tables V and VI contain the amplitudes of the most important $|(j^2)J, (p\bar{h})J; 0\rangle$ core admixtures in the $|(j^2)0^+\rangle$ model space configurations for ^{50}Ti ($j = 1f_{7/2}$) and ^{90}Zr ($J = 1g_{9/2}$). These tables contain all the information needed to describe the $|(j^2)0^+\rangle \rightarrow |(j^2)J^+\rangle$ transitions in these nuclei, since the amplitudes of the $|(j^2)0, (p\bar{h})J; J\rangle$ core admixtures in the $|(j^2)J^+\rangle$ are easily obtained from the given amplitudes by means of Eq. (76).

It is apparent from the tables that the number of core admixtures that make important contributions are not large in comparison to the total num-

ber of allowed admixtures. There are two factors which limit the number of configurations which make important contributions. The first is the requirement of good overlap between the radial wave functions for the p-h pair and the active valence particles, e.g., see the discussion in Sec. IIID. The second is that $|(j^2)J, (p\bar{h})J; 0\rangle$ admixtures where the p and h orbits are coplanar are heavily favored. This condition, which may be stated

$$|l_p \pm l_h| = J,$$

is a property of the reduced matrix elements $\langle j_p \| T^{J0J} \| j_h \rangle$ which enter in the calculation of the J th multipole coefficient of the coupling interaction, e.g., see Eq. (85) for the multipole coefficient in the zero-range limit. The same $|(j^2)J, (p\bar{h})J, 0\rangle$ admixtures which mix strongly with the $|(j^2)0^+\rangle$ configurations also produce the largest matrix elements of \mathcal{T} because the latter, Eq. (77), are also proportional to $\langle j_p \| T^{J0J} \| j_h \rangle$. These points are summarized explicitly in the zero-range expression for the matrix elements of

TABLE V. Core admixtures in ground state of ^{50}Ti .

$p\bar{h}$	$\epsilon(\text{ph})$ (MeV)	$\alpha((1f_{7/2})^2J, (p\bar{h})J; 0 (1f_{7/2})^2 0)^a$					
		Protons			Neutrons		
		$J=2$	$J=4$	$J=6$	$J=2$	$J=4$	$J=6$
$1g_{9/2}-1d_{5/2}^{-1}$	15.5	-0.06	-0.02	-0.01	-0.19	-0.10	-0.05
		-0.22	-0.08	-0.03	-0.26	-0.13	-0.06
$1g_{7/2}-1d_{3/2}^{-1}$	17.7	-0.05	-0.03		-0.14	-0.07	
		-0.17	-0.07		-0.19	-0.09	
$1f_{5/2}-1p_{1/2}^{-1}$	20.9	-0.04					
		-0.08					
$2p_{3/2}-1f_{7/2}^{-1}$	4.8				0.30	0.15	
					0.38	0.15	
$1f_{5/2}-1f_{7/2}^{-1}$	8.8				-0.11	-0.14	-0.16
					-0.16	-0.17	-0.16
$1g_{9/2}-2s_{1/2}^{-1}$	14.3		-0.03			-0.10	
			-0.07			-0.11	
$1g_{7/2}-2s_{1/2}^{-1}$	19.3		0.02			0.06	
			0.04			0.07	
$1g_{9/2}-1d_{3/2}^{-1}$	12.7		-0.04	-0.04		-0.07	-0.09
			-0.09	-0.09		-0.09	-0.12
$1g_{7/2}-1d_{5/2}^{-1}$	20.5	0.01	0.02	0.02	0.04	0.05	0.06
		0.04	0.05	0.05	0.06	0.07	0.08
$1f_{5/2}-1p_{3/2}^{-1}$	22.5	0.02	0.03		0.05	0.07	
		0.03	0.04		0.06	0.08	
$2p_{1/2}-1f_{7/2}^{-1}$	6.8					-0.12	
						-0.14	
$1f_{7/2}-1p_{3/2}^{-1}$	18.0	-0.04	-0.01				
		-0.11	-0.01				
$1f_{7/2}-1p_{1/2}^{-1}$	16.4		-0.03				
			-0.06				

^aThe first entry for a given $p\bar{h}$ and J is the amplitude obtained using first order perturbation theory and the second entry is the amplitude obtained using the renormalized coupling interaction.

TABLE VI. Core admixtures in $(1g_{9/2}^2)$ configuration in ^{90}Zr .

$\bar{p}\bar{h}$	$\epsilon(\text{ph})$ (MeV)	$\alpha((1g_{9/2}^2)J, (\bar{p}\bar{h})J; 0 (1g_{9/2}^2)0)^a$							
		Protons				Neutrons			
		$J=2$	$J=4$	$J=6$	$J=8$	$J=2$	$J=4$	$J=6$	$J=8$
$1h_{11/2}-1f_{7/2}^{-1}$	12.5	-0.06	-0.02	-0.01	-0.00	-0.17	-0.10	-0.06	-0.03
		-0.22	-0.08	-0.04	-0.00	-0.25	-0.13	-0.08	-0.04
$1h_{9/2}-1f_{5/2}^{-1}$	14.5	-0.05	-0.03	-0.02		-0.13	-0.07	-0.04	
		-0.17	-0.08	-0.04		-0.19	-0.10	-0.05	
$1g_{7/2}-1d_{3/2}^{-1}$	15.0	-0.05	-0.03			-0.12	-0.06		
		-0.12	-0.05			-0.15	-0.07		
$2f_{7/2}-2p_{3/2}^{-1}$	15.0	-0.01	-0.01			-0.04	-0.02		
		-0.11	-0.04			-0.09	-0.04		
$1i_{13/2}-1g_{9/2}^{-1}$	13.0					-0.16	-0.10	-0.06	-0.04
						-0.24	-0.11	-0.05	-0.01
$2d_{5/2}-1g_{9/2}^{-1}$	4.5					0.21	0.12	0.07	
						0.31	0.13	0.05	
$1h_{11/2}-1f_{5/2}^{-1}$	9.5		-0.04	-0.04	-0.03		-0.06	-0.07	-0.08
			-0.08	-0.07	-0.07		-0.07	-0.09	-0.10
$1h_{11/2}-2p_{3/2}^{-1}$	10.5		-0.04	-0.01			-0.11	-0.05	
			-0.08	-0.03			-0.13	-0.06	
$1g_{7/2}-1d_{5/2}^{-1}$	17.0	0.01	0.02	0.02		0.03	0.04	0.06	
		0.02	0.03	0.01		0.04	0.05	0.07	
$1g_{7/2}-2s_{1/2}^{-1}$	16.0		0.02				0.06		
			0.03				0.07		
$1i_{13/2}-1d_{5/2}^{-1}$	26.0		0.02	0.01	0.00		0.04	0.02	0.01
			0.04	0.00	-0.01		0.06	0.02	0.00
$1h_{9/2}-2p_{1/2}^{-1}$	14.0						-0.06		
							-0.08		
$1g_{7/2}-1g_{9/2}^{-1}$	7.2					-0.07	-0.10	-0.10	-0.12
						-0.12	-0.13	-0.12	-0.12
$1h_{9/2}-1f_{7/2}^{-1}$	17.5	0.00	0.02	0.02	0.02	0.03	0.04	0.04	0.04
		0.03	0.04	0.04	0.04	0.04	0.05	0.05	0.06
$1h_{9/2}-2p_{3/2}^{-1}$	15.5		0.01	0.02			0.03	0.05	
			0.03	0.04			0.04	0.06	
$1i_{13/2}-2s_{1/2}^{-1}$	25.0			0.01				0.03	
				0.01				0.03	
$1h_{11/2}-2p_{1/2}^{-1}$	9.0							-0.08	
								-0.09	
$2d_{3/2}-1g_{9/2}^{-1}$	6.5						-0.05	-0.08	
							-0.07	-0.09	
$1i_{13/2}-1d_{3/2}^{-1}$	24.0			0.01	0.01			0.02	0.02
				0.02	0.01			0.02	0.02
$2p_{1/2}-2p_{3/2}^{-1}$	3.5	-0.10							
		-0.37							
$2p_{1/2}-1f_{5/2}^{-1}$	4.0	0.10							
		0.24							
$1g_{9/2}-1d_{5/2}^{-1}$	13.5	-0.04	-0.01	-0.01					
		-0.14	-0.02	0.02					
$2p_{1/2}-1f_{7/2}^{-1}$	5.5		-0.06						
			-0.12						
$1g_{9/2}-2s_{1/2}^{-1}$	12.5		-0.03						
			-0.04						
$1g_{9/2}-1d_{3/2}^{-1}$	11.5		-0.03	-0.03					
			-0.06	-0.05					

^aThe first entry for a given $\bar{p}\bar{h}$ and J is the amplitude obtained using first order perturbation theory and the second entry is the amplitude obtained using the renormalized coupling interaction.

τ , Eqs. (88)–(91), where it is seen that dominant terms are proportional to

$$\langle j_p \| T^{J\sigma J} \| j_h \rangle^2 I(l_p l_\alpha l_h l_\gamma).$$

We also note that the amplitudes for some of the positive parity $1\hbar\omega$ excitations are quite large, particularly in the calculations where \bar{G}' has been used. Our estimate of these large admixtures is undoubtedly unreliable and it would appear necessary to include the second order terms in estimating $\delta\tau$ to improve this situation. Additional indications that the second order terms may be important in some cases will be seen in the next section.

Agassi and Schaeffer¹⁶ have previously reported the results of a first order estimate of the effect of core polarization in the excitation of 2^+ states in various nuclei. The $0^+ \rightarrow 2^+$ transition in ^{90}Zr is the only point of overlap between the calculations of Ref. 16 and the present work. Agassi and Schaeffer obtained a particularly small core polarization effect in this case while we obtain a large effect as will be seen in the next section. From their published amplitudes we find that the core coupling interaction they have used is quite similar to the KK force used in the present work; however, we note that they have used a much smaller excluded space than we have (all $2\hbar\omega$ excitations) and thus they have missed several important core admixtures.

C. Radial transition densities and radial form factors

Before examining the (e, e') form factors and (p, p') differential cross sections which are the final results of this paper, it is useful to discuss the radial transition densities and radial form factors which provide the link between the wave functions described in the preceding section and these final results. The radial transition densities and the radial form factors were defined in Sec. II. These functions are the matrix elements of the one-body operators for which we are calculating the renormalization due to core polarization.

The $LSJ = 202$ transition densities for $0^+ \rightarrow 2^+$ transitions in ^{50}Ti and ^{90}Zr , the $1h_{9/2} - 2f_{7/2}$ transition in ^{209}Bi , and the $3p_{1/2} - 2f_{5/2}$ transition in ^{207}Pb are shown in Fig. 4. The valence transition densities as well as the complete proton and neutron transition densities [$D + C(p)$ and $D + C(n)$] obtained with core polarization included are shown in each case. We have shown the results obtained using the renormalized core coupling interaction, although for our purposes here the first order results would have served equally well. For the first three transitions the valence transition den-

sities have shapes which are very similar to the complete proton and neutron transition densities. This is a typical feature of the transition densities obtained for most of the transitions considered in this work. It was anticipated in the overlap argument used in the discussion of the enhancement and retardation effects due to core polarization given in Sec. III D. The results for the $3p_{1/2} - 2f_{5/2}$ transition in ^{207}Pb is a case where the differences in shape between the valence transition densities and the complete proton and neutron transition densities are the largest. Even here the differences are not too great in the important surface region.

The radial form factors obtained by averaging the real part of \bar{V} over the transition densities of Fig. 4 are shown in Fig. 5. The distributions in Fig. 5 are quite similar to those shown in Fig. 4, except that the neutron functions are increased in size relative to the proton functions. This occurs because $\bar{V}_{pn}^0 \approx 3\bar{V}_{pp}^0$. The main point is that the projectile-target interaction acts much like an overall scaling factor for the transition densities. Because of the finite range of this interaction the averaging does tend to smear out the transition densities slightly. This has the effect of reducing, to some degree, the importance of any shape differences between the various transition density functions.

The above discussion suggests that the results for the (e, e') and (p, p') reactions can be quali-

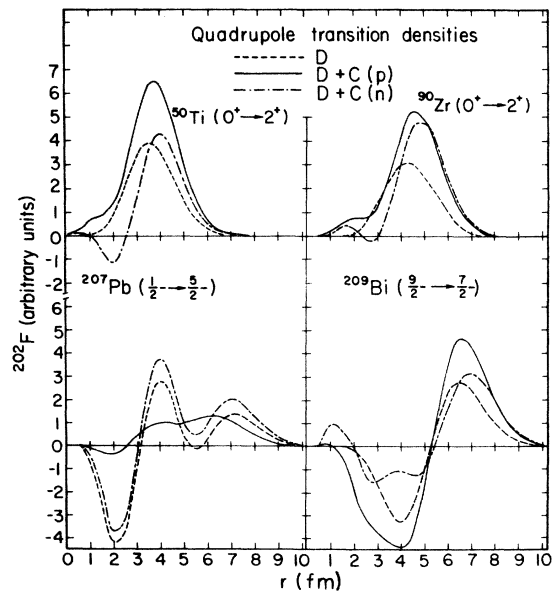


FIG. 4. Transition densities for $L = 2$ transitions in ^{50}Ti , ^{90}Zr , ^{207}Pb , and ^{209}Bi .

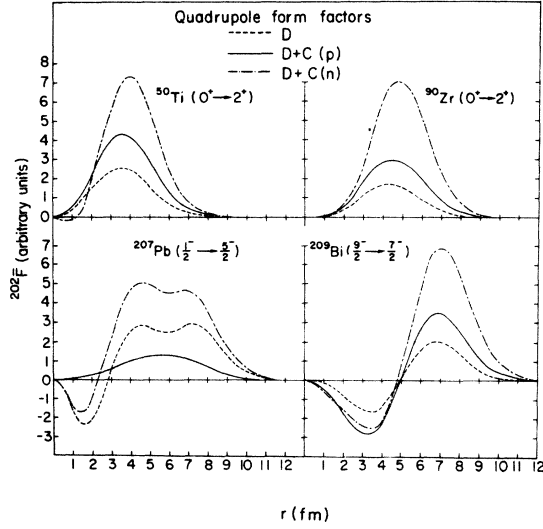


FIG. 5. Form factors obtained from transition densities of Fig. 4.

tatively understood by comparing the relative magnitudes of a single moment of the various transition density functions, most logically the lowest moment, and by introducing appropriate scaling factors which are characteristic of these reactions. For (p, p') the scaling factors are the relative strengths of the various components of the projectile-target interaction and for (e, e') the scaling factors are the nucleon charges, i.e., $e_p = 1$ and $e_n = 0$. A comparison of this type is useful, because it allows the general features of the results to be displayed in a transparent and compact form. The (p, p') differential cross sections and (e, e') form factors do show some sensitivity to higher moments of the transition densities,¹⁴ so any fine details in the results can only be seen by calculating these quantities as prescribed in Sec. II. These final results will be shown in the next section, after we make this rough comparison.

To make this comparison in cases where there are valence protons, we divide the complete proton transition density into valence and core parts and introduce the parameters

$$\lambda_p^{LSJ} = \frac{\int_0^\infty F_{p_c}^{LSJ}(r) r^{L+2} dr}{\int_0^\infty F_{p_v}^{LSJ}(r) r^{L+2} dr}, \quad (95)$$

$$\lambda_n^{LSJ} = \frac{\int_0^\infty F_n^{LSJ}(r) r^{L+2} dr}{\int_0^\infty F_{p_v}^{LSJ}(r) r^{L+2} dr} \quad (96)$$

which measure the contribution to the nuclear transition densities from core polarization relative to the valence transition density. We then assume that the effect of core polarization on the

(p, p') cross sections can be adequately characterized by the enhancement factor which was introduced in Eq. (62). In terms of λ_p^{LSJ} and λ_n^{LSJ} this factor is approximately given by

$$\epsilon_p^{LSJ}(p) = 1 + \lambda_p^{LSJ} + \alpha_S \lambda_n^{LSJ}, \quad (97)$$

where $\alpha_S = V_{pn}^S / V_{pp}^S$. In a similar fashion we introduce the effective charge

$$e_{\text{eff}}^{Jp} = 1 + \lambda_p^{J0J} \quad (98)$$

to characterize the effect of core polarization on the (e, e') form factors. The effective charge has precise meaning for inelastic electron scattering in the low q limit, corresponding to γ decay, because only the lowest moment of the proton transition densities come into consideration here. This was pointed out at the end of Sec. IIB. In cases where there are valence neutrons the definitions of λ_p^{LSJ} and λ_n^{LSJ} are modified:

$$\lambda_p^{LSJ} = \frac{\int_0^\infty F_p^{LSJ}(r) r^{L+2} dr}{\int_0^\infty F_{n_v}^{LSJ}(r) r^{L+2} dr}, \quad (99)$$

$$\lambda_n^{LSJ} = \frac{\int_0^\infty F_{n_c}^{LSJ}(r) r^{L+2} dr}{\int_0^\infty F_{n_v}^{LSJ}(r) r^{L+2} dr} \quad (100)$$

and

$$\epsilon_p^{LSJ}(n) = 1 + \alpha_S^{-1} \lambda_p^{LSJ} + \lambda_n^{LSJ}, \quad (101)$$

$$e_{\text{eff}}^{Jn} = \lambda_p^{J0J}. \quad (102)$$

As it is sometimes convenient to talk in terms of the isoscalar and isovector contributions to $\epsilon_p^{LSJ}(q)$ and e_{eff}^{Jq} , it is also useful to give Eqs. (97), (98), (101), and (102) in terms of these quantities. These expressions are

$$\epsilon_p^{LSJ}(q) = 1 + \alpha_S^0(q) \lambda_0^{LSJ} + \alpha_S^1(q) \lambda_1^{LSJ}, \quad (103)$$

$$e_{\text{eff}}^{Jq} = e_q + \frac{1}{2} (\lambda_0^{J0J} + \lambda_1^{J0J}), \quad (104)$$

where

$$\lambda_0^{LSJ} = \lambda_p^{LSJ} + \lambda_n^{LSJ}, \quad \lambda_1^{LSJ} = \lambda_p^{LSJ} - \lambda_n^{LSJ}, \quad (105)$$

$$\alpha_S^0(q) = \frac{1}{2} (V_{pp}^S + V_{pn}^S) / V_{pq}^S, \quad (106)$$

$$\alpha_S^1(q) = \frac{1}{2} (V_{pp}^S - V_{pn}^S) / V_{pq}^S.$$

Equations analogous to those just given have previously been used by Atkinson and Madsen²² to compute enhancement factors for normal parity transitions in (p, p') scattering from known effective charges. They assumed isoscalar coupling and so took $\lambda_p^{J0J} = \lambda_n^{J0J}$. Using these relations in this manner is quite similar to the application of the schematic model made by Love and Satchler.¹⁵ These relations might also be used as the basis for a phenomenological study of the available experimental data. Schaeffer²³ has used scaling

factors, similar to the λ_q^{LSJ} introduced here, in a study of some experimental (p, p') and γ -decay for collective excitations in various nuclei. The purpose of this study was to gain information about the relationship between the proton and neutron transition densities for transition of this type. In the present work we obtain λ_p^{LSJ} and λ_n^{LSJ} directly from the calculations and this scheme is only being used to summarize our results.

Table VII contains the results we have obtained using first order perturbation theory for all of the allowed $S=0$ transition densities which occur in the cases being considered. The parameters, λ_p^{J0J} , λ_n^{J0J} , λ_0^{J0J} , and λ_1^{J0J} are shown in each case with the corresponding values of ϵ_p^{J0J} and e_{eff}^J computed according to Eqs. (97), (98), (101), and

(102) or the equivalent relations Eqs. (103)–(106). In these computations we have used $\alpha_0 = 2.75$ which is satisfactory for our choice of \bar{V} as was discussed in Sec. IIA 2. Corresponding to this value for α_0 , we have $\alpha_0^0(p) = 1.88$, $\alpha_0^1(p) = -0.88$, $\alpha_0^0(n) = 0.68$, and $\alpha_0^1(n) = -0.32$ in the isospin notation.

Also shown in Table VII are values of ϵ_p^{J0J} and e_{eff}^J which have been estimated from the available experimental data. The experimental values of ϵ_p^{J0J} have been obtained by taking the square roots of the ratios of the experimental and theoretical valence integrated cross sections. Only the real part of \bar{V} has been used in calculating the theoretical valence cross sections as we wish to keep separate the effect of the imaginary part of \bar{V}

TABLE VII. Parameters for $S=0$ transition densities from first order calculations.

Target	Transition J_f^{π} ($J_0 J$)	λ_p^{J0J}	λ_n^{J0J}	λ_0^{J0J}	λ_1^{J0J}	Theory ^a		Experiment ^a	
						e_{eff}^J	ϵ_p^{J0J}	e_{eff}^J	ϵ_p^{J0J}
⁴² Ca	2 ⁺ (202)	0.68	0.23	0.91	0.45	0.68	1.47	1.7 ± 0.1 ^b	2.03 ^c
	4 ⁺ (404)	0.48	0.17	0.65	0.31	0.48	1.34	...	2.12 ^c
	6 ⁺ (606)	0.22	0.08	0.30	0.14	0.22	1.16
⁵⁰ Ti	2 ⁺ (202)	0.22	0.88	1.10	-0.66	1.22	3.65	1.7 ± 0.2 ^d	5.34 ^e
	4 ⁺ (404)	0.16	0.70	0.86	-0.54	1.16	3.09	1.4 ± 0.1 ^f	4.86 ^e
	6 ⁺ (606)	0.07	0.43	0.50	-0.36	1.07	2.25
⁸⁸ Y	$\frac{9}{2}^+$ (505)	0.28	0.74	1.02	-0.46	1.28	3.32
⁹⁰ Zr	2 ⁺ (202)	0.31	1.22	1.53	-0.91	1.31	4.92	2.8 ± 0.4 ^g	6.45 ^h
	4 ⁺ (404)	0.23	0.97	1.20	-0.74	1.23	3.90	2.1 ± 0.3 ⁱ	5.39 ^h
	6 ⁺ (606)	0.12	0.74	0.86	-0.62	1.12	3.16	...	4.94 ^h
	8 ⁺ (808)	0.08	0.45	0.53	-0.37	1.08	2.54	...	6.35 ^h
	5 ⁻ (505)	0.28	0.74	1.02	-0.46	1.28	3.32	1.4 ± 0.1 ^j	4.55 ^h
²⁰⁷ Pb	$\frac{5}{2}^-$ (202)	0.62	0.38	1.00	0.24	0.62	1.60	0.93 ± 0.01 ^k	2.50 ^l
	$\frac{3}{2}^-$ (202)	0.58	0.36	0.94	0.22	0.58	1.57	0.75 ± 0.02 ^k	1.91 ^l
	$\frac{13}{2}^+$ (707)	0.39	0.32	0.71	0.07	0.39	1.46	...	3.07 ^l
	$\frac{1}{2}^-$ (404)	0.61	0.39	1.00	0.22	0.61	1.61	...	2.63 ^l
²⁰⁹ Bi	$\frac{1}{2}^-$ (202)	0.38	1.25	1.63	-0.87	1.38	4.82	2.3 ± 0.6 ^m	...
	(404)	0.33	1.22	1.55	-0.89	1.33	4.68
	(606)	0.26	1.16	1.42	-0.90	1.26	4.44
	(808)	0.18	1.00	1.18	-0.82	1.18	3.93
	$\frac{13}{2}^+$ (303)	0.38	1.32	1.70	-0.94	1.38	5.01	5.3 ± 0.7 ⁿ	24.0 ^o
	(505)	0.24	1.10	1.34	-0.86	1.24	4.27
	(707)	0.14	0.81	0.95	-0.67	1.14	3.38
	(909)	0.08	0.53	0.61	-0.45	1.08	2.54
(11 011)	0.01	0.37	0.38	-0.36	1.01	2.03	

^aSee text for comments on the manner in which the numbers listed in these columns have been obtained.

^bSee Refs. 54 and 55.

^cSee Ref. 56.

^dSee Refs. 54 and 57–59.

^eSee Refs. 44 and 45.

^fSee Refs. 54 and 58.

^gSee Refs. 58–61.

^hSee Refs. 18, 39, and 46.

ⁱSee Ref. 58.

^jSee Refs. 62 and 63.

^kSee Ref. 64.

^lSee Refs. 42 and 65.

^mSee Refs. 66 and 67.

ⁿSee Refs. 66–68.

^oSee Ref. 17.

which will be discussed later. The experimental data were taken from the references indicated in the table and the experimental integrated cross sections have been determined by normalizing the results of distorted-wave Born approximation collective model calculations⁶⁹ to the experimental differential cross sections. For transitions where data are available at more than one incident proton energy, the experimental ϵ_p^{J0J} shown are average values. In all but a few instances the experimental ϵ_p^{J0J} were found to be nearly energy independent. The optical model parameters used in calculating the collective model cross sections and the theoretical valence cross sections have been taken from the same references where the experimental data were found. Most of these parameter sets have been included in Table XII. For $2p_{1/2} \rightarrow 1g_{9/2}$ transition in ⁸⁹Y and the $1h_{9/2} \rightarrow 2f_{7/2}$ transition in ²⁰⁹Bi it was not possible to determine the experimental ϵ_p^{J0J} because more than one *LSJ* transfer is observed to contribute to the experimental cross

section in these cases.

The references containing the data which were used to determine the experimental values of e_{eff}^J are also shown in Table VII. Generally there was more than one piece of data available for each determination. For transitions where electron scattering data were available two methods were used to extract the experimental effective charge. One of these methods was to determine e_{eff}^J from the values of $B(EJ\uparrow)$ obtained from transition densities which were fitted to the experimental form factors. The second method was to normalize the peak value of theoretical valence form factors to the peak value of the experimental form factors. It has been suggested⁷⁰ that the second method is somewhat more reliable than the first. The sensitivity of the experimental effective charges to the theoretical radial wave functions was also checked. In most cases the changes in the effective charge due to reasonable changes in the radial wave functions were well within the variations

TABLE VIII. Parameters for $S=0$ transition densities obtained using renormalized coupling interaction.

Target	Transition J_f^{π} (J0J)	λ_p^{J0J}	λ_n^{J0J}	λ_0^{J0J}	λ_1^{J0J}	Theory ^a		Experiment ^a	
						e_{eff}^J	ϵ_p^{J0J}	e_{eff}^J	ϵ_p^{J0J}
⁴² Ca	2 ⁺ (202)	0.98	0.83	1.81	0.15	0.98	2.18	1.7 ± 0.1	2.03
	4 ⁺ (404)	0.61	0.41	1.02	0.20	0.61	1.62	...	2.12
	6 ⁺ (606)	0.25	0.14	0.39	0.11	0.25	1.23
⁵⁰ Ti	2 ⁺ (202)	0.81	1.36	2.17	-0.55	1.81	5.61	1.7 ± 0.2	5.34
	4 ⁺ (404)	0.40	0.90	1.30	-0.50	1.40	3.95	1.4 ± 0.1	4.86
	6 ⁺ (606)	0.18	0.49	0.67	-0.31	1.18	2.53
⁸⁹ Y	$\frac{9}{2}^+$ (505)	0.35	0.79	1.14	-0.44	1.35	3.52
⁹⁰ Zr	2 ⁺ (202)	1.30	2.07	3.37	-0.77	2.30	7.95	2.8 ± 0.4	6.45
	4 ⁺ (404)	0.66	1.37	2.06	-0.71	1.69	5.43	2.1 ± 0.3	5.39
	6 ⁺ (606)	0.33	0.89	1.25	-0.56	1.33	3.78	...	4.94
	8 ⁺ (808)	0.16	0.49	0.76	-0.33	1.16	2.51	...	6.35
	5 ⁻ (505)	0.35	0.79	1.14	-0.44	1.35	3.52	1.4 ± 0.1	4.55
²⁰⁷ Pb	$\frac{5}{2}^-$ (202)	0.85	1.10	1.95	-0.25	0.85	2.41	0.93 ± 0.01	2.50
	$\frac{3}{2}^-$ (202)	0.87	1.20	2.07	-0.33	0.87	2.51	0.75 ± 0.02	1.91
	$\frac{13}{2}^+$ (707)	0.41	0.59	1.00	-0.18	0.41	1.74	...	3.07
	$\frac{7}{2}^-$ (404)	0.78	0.82	1.60	-0.04	0.78	2.10	...	2.63
²⁰⁹ Bi	$\frac{7}{2}^-$ (202)	0.87	1.63	2.50	-0.76	1.87	6.35	2.3 ± 0.6	...
	(404)	0.80	1.65	2.45	-0.85	1.80	6.34
	(606)	0.60	1.39	1.99	-0.79	1.60	5.42
	(808)	0.36	1.06	1.42	-0.70	1.36	4.28
	$\frac{13}{2}^+$ (303)	0.14	1.42	1.56	-1.28	1.14	5.05	5.3 ± 0.7	24.0
	(505)	0.14	1.05	1.19	-0.91	1.14	4.03
	(707)	0.12	0.68	0.80	-0.56	1.12	2.99
	(909)	0.05	0.49	0.54	-0.44	1.05	2.39
	(11011)	0.02	0.35	0.37	-0.33	1.02	1.98

^a See text for comments on the manner in which the numbers listed in these columns have been obtained. References for experimental values have been given in Table VII.

noted in the experimental data. An exception to this is the $1h_{9/2} - 2f_{7/2}$ transition in ^{209}Bi where harmonic oscillator radial wave functions and finite well wave functions⁷¹ produced values for e_{eff}^2 which differed by nearly a factor of 2. The experimental values for e_{eff}^J shown in Table VII are averages of the values determined from the various sets of experimental data according to the methods described above. The uncertainties shown are average deviations which are mainly due to fluctuations in the experimental data.

Table VIII contains a summary of the results we have obtained for the $S=0$ transition densities in the calculations using the renormalized core coupling interaction of Eq. (67). The format of this table is identical to that of Table VII.

The results obtained for the $S=1$ transition densities using first order perturbation theory are shown in Table IX. In calculating the theoretical values of ϵ_p^{L1J} , it was assumed that $\alpha_1 = -0.20$ which corresponds to $\alpha_1^0(p) = 0.40$, $\alpha_1^1(p) = 0.60$, $\alpha_1^0(n) = -2.00$, and $\alpha_1^1(n) = -3.00$. These are again satisfactory for our choice of \bar{V} . No experimental values for ϵ_p^{L1J} are shown because $S=1$ amplitudes were not found to be dominant in any of the transitions which we have considered. The results for the $S=1$ transition densities obtained using \bar{G}' for the core coupling interaction do not differ greatly from the first order results; therefore, they have not been shown. The differences are small because we have assumed that $\bar{G}' - G$ is spin independent. Even if the appropriate spin dependence had been included in $\bar{G}' - G$, the results would not have been effected greatly. The main thing to notice in Table IX is the retardation of the $S=1$ amplitudes compared to the enhancement of the $S=0$ amplitudes apparent from Tables VII and VIII.

From Table VII we see that the first order calculations predict important core polarization corrections for the $S=0$ amplitudes, even for the highest multipoles considered. In all cases, however, the correction falls somewhat short of experiment. The most notable feature of these calculations is that they predict a large isovector component in the $S=0$ transition densities. This is not borne out experimentally for the transition where both electromagnetic and proton scattering data are available. This may be seen by comparing the theoretical and experimental results for the polarization charge ($\delta e_{\text{eff}}^J = \lambda_p^{J0J}$) and the corresponding factor for proton scattering ($\delta \epsilon_p^{J0J} = \epsilon_p^{J0J} - 1$). For the cases where there are valence protons the first order calculations give a better estimate of $\delta \epsilon_p^{J0J}$ than they do of δe_{eff}^J while the reverse is true for the transition involving valence neutrons.

From Table VIII we see that the main effect of interactions in the excluded space, as determined by our calculations using \bar{G}' as the core coupling interaction, is to increase the isoscalar components of the $S=0$ transition densities relative to the isovector components which in turn brings improved agreement with experiment. The magnitude of this effect decreases with increasing

TABLE IX. Parameters for $S=1$ transition densities obtained from first order calculations.

Target	J_f^*	(L1J)	λ_p^{L1J}	λ_n^{L1J}	λ_0^{L1J}	λ_1^{L1J}	ϵ_p^{L1J}	
^{89}Y	$\frac{3}{2}^*$	(314)	-0.45	0.08	-0.37	-0.53	0.53	
		(514)	-0.28	0.05	-0.23	-0.33	0.71	
		(515)	-0.25	0.05	-0.20	-0.30	0.74	
^{90}Zr	5^-	(515)	-0.25	0.05	-0.20	-0.30	0.74	
^{207}Pb	$\frac{5}{2}^-$	(212)	0.05	-0.41	-0.36	0.46	0.34	
		(213)	0.03	-0.32	-0.29	0.35	0.53	
		(413)	0.04	-0.27	-0.23	0.31	0.53	
	$\frac{3}{2}^-$	(011)	0.05	-0.20	-0.15	0.25	0.55	
		(211)	0.09	-0.44	-0.35	0.53	0.11	
	$\frac{1}{2}^*$	(212)	0.06	-0.39	-0.33	0.45	0.31	
		(516)	0.05	-0.45	-0.40	0.50	0.30	
		(716)	0.02	-0.11	-0.09	0.13	0.79	
	$\frac{1}{2}^-$	(717)	0.03	-0.29	-0.26	0.32	0.56	
		(213)	0.06	-0.42	-0.36	0.48	0.28	
		(413)	0.08	-0.34	-0.26	0.42	0.26	
	^{208}Bi	$\frac{7}{2}^-$	(414)	0.06	-0.38	-0.32	0.44	0.32
			(011) ^a
			(211)	-0.28	0.06	-0.22	-0.34	0.71
			(212)	-0.38	0.09	-0.29	-0.47	0.61
(213)			-0.40	0.11	-0.29	-0.51	0.58	
(413)			-0.23	0.09	-0.14	-0.32	0.76	
(414)			-0.32	0.10	-0.22	-0.42	0.66	
(415)			-0.38	0.11	-0.27	-0.49	0.60	
(615)			-0.16	0.09	-0.07	-0.25	0.82	
(616)			-0.25	0.09	-0.16	-0.34	0.73	
(617)			-0.33	0.11	-0.22	-0.44	0.65	
(817)			-0.09	0.08	-0.01	-0.17	0.90	
(818)			-0.17	0.09	-0.08	-0.26	0.84	
$\frac{1}{2}^*$			(112)	-0.33	0.10	-0.23	-0.43	0.65
			(312)	-0.22	0.09	-0.13	-0.31	0.77
	(313)	-0.30	0.11	-0.19	-0.41	0.68		
	(314)	-0.29	0.11	-0.18	-0.40	0.69		
	(514)	-0.21	0.09	-0.22	-0.30	0.88		
	(515)	-0.22	0.10	-0.12	-0.32	0.77		
	(516)	-0.23	0.09	-0.14	-0.32	0.75		
	(716)	-0.13	0.08	-0.05	-0.21	0.86		
	(717)	-0.13	0.08	-0.05	-0.21	0.86		
	(718)	-0.16	0.06	-0.10	-0.22	0.83		
(918)	-0.04	0.06	0.02	-0.01	0.94			
(919)	-0.07	0.05	-0.02	-0.12	0.92			
(9110)	-0.13	0.03	-0.10	-0.16	0.87			
(11110)	0.00	0.04	0.04	-0.04	0.99			
(11111)	-0.04	0.03	-0.01	-0.07	0.95			

^aThe valence transition is strictly forbidden in this case so λ^{011} cannot be defined. Core polarization does not break this selection rule to any great extent.

TABLE X. Comparison of the results of this work (PW) for some quadrupole transitions with results obtained previously by Siegal and Zamick (SZ).

Core	Transition	PW(G_{KK}) ^a		SZ(G_{KK}) ^b		PW(\bar{G}') ^a		SZ(TDA) ^b	
		λ_0^{202}	λ_1^{202}	λ_0^{202}	λ_1^{202}	λ_0^{202}	λ_1^{202}	λ_0^{202}	λ_1^{202}
⁴⁰ Ca	$1f_{7/2} \rightarrow 1f_{7/2}$	0.91	+0.45	0.80	+0.38	1.81	+0.15	1.86	+0.30

^aPW denotes present work. G_{KK} refers to first order calculations and \bar{G}' refers to calculations with renormalized coupling interaction.

^bSZ denotes Siegal and Zamick (Ref. 10). TDA refers to the treatment of excluded space interactions in the TDA approximation.

multipolarity. In Table X we compare the results of our first order calculations and our calculation using \bar{G}' with the first order and TDA results of Siegal and Zamick¹⁰ for $LSJ=202$ and the $1f_{7/2} \rightarrow 1f_{7/2}$ neutron transition assuming a ⁴⁰Ca core. We conclude that our result obtained using G' is consistent with the estimate of excluded space interactions using the TDA. It was not possible to make a similar comparison for any of the higher multipoles we have considered; however, the decrease in the importance of excluded space interactions with increasing multipolarity, predicted by our calculations with \bar{G}' , is consistent with the results of TDA and RPA calculations⁴² for closed shell cores which indicate that the collectivity of core excitations decrease with increasing multipolarity.

Although the results obtained with \bar{G}' are a definite improvement over the first order results for $\delta\mathcal{T}$, some important discrepancies still appear in Table XI. One is that the theoretical values of ϵ_p^{j0j} fall off somewhat faster with increasing multipole than do the experimental values. In the next section it will be seen that this discrepancy is removed when the imaginary part of \bar{V} is introduced.

Another discrepancy is the relatively poor values obtained for the effective charge in the case of the

$0^+ \rightarrow 2^+$ transitions in ⁴²Ca and ⁹⁰Zr while the theoretical e_{eff}^2 for the $0^+ \rightarrow 2^+$ transition in ⁵⁰Ti appears to be adequate. The $B(E2)$ for the $6^+ \rightarrow 4^+$ transitions in ⁴²Ca and ⁵⁰Ti and the $8^+ \rightarrow 6^+$ transition in ⁹⁰Zr have been determined experimentally.^{59,72} The experimental values of e_{eff}^2 for these transitions are compared with the theoretical results we have obtained using G and \bar{G}' in Table XI. We note that our model for core polarization predicts that e_{eff}^2 for the transitions between the two upper states of a (j^2) configuration should be the same as for the $0^+ \rightarrow 2^+$ transition. This is borne out by the data only in the case of ⁵⁰Ti. For ⁴²Ca our theoretical result for e_{eff}^2 is in quite good agreement with the experimental value for the $6^+ \rightarrow 4^+$ transition which is only about half the value required for the $0^+ \rightarrow 2^+$ transition. Experimentally the situation is about the same for ⁹⁰Zr. We conclude that it is necessary to include second order terms in estimating $\delta\mathcal{T}$ in order to resolve these discrepancies. This is consistent with the suggestion of others^{73,74} that 4p-2h admixtures are important in ⁴²Ca and ⁹⁰Zr.

The final discrepancy we note is that the calculations fail to reproduce the large values of e_{eff}^3 and ϵ_p^{303} required to explain the $1h_{9/2} \rightarrow 1i_{3/2}$ transition in ²⁰⁹Bi. It is well known⁴⁷ that there are important contributions to this transition from

TABLE XI. Effective charges for some quadrupole transitions not considered in Tables II, VII, and VIII.

Nuclide	Transition	Theory		Experiment e_{eff}^2
		$e_{\text{eff}}^2(G_{\text{KK}})$	$e_{\text{eff}}^2(\bar{G}')$	
⁴² Ca	$6^+ \rightarrow 4^+$	0.68	0.98	0.8 ± 0.1 ^a
⁵⁰ Ti	$6^+ \rightarrow 4^+$	1.22	1.81	1.8 ± 0.3 ^a
⁹⁰ Zr	$8^+ \rightarrow 6^+$	1.31	2.30	2.1 ± 0.1 ^b
²⁰⁸ Pb + p	$1h_{9/2} \rightarrow 1h_{9/2}$	1.35	2.27	1.5 ± 0.1 ^c
²⁰⁸ Pb + n	$3d_{5/2} \rightarrow 2s_{1/2}$	0.37	0.55	(0.42 ± 0.01) ^c
	$2g_{9/2} \rightarrow 2g_{9/2}$	0.36	1.04	(0.84 ± 0.07) ^c
²⁰⁸ Pb + n^{-1}	$1i_{13/2} \rightarrow 1i_{13/2}$	0.81	1.22	(0.96 ± 0.04) ^c

^aSee Ref. 72.

^bSee Ref. 59.

^cSee Ref. 64.

admixture of low-lying particle-vibration states in the single particle states, i.e., $|1h_{9/2} \times 3^-; \frac{13}{2}\rangle$ and $|1i_{13/2} \times 3^-; \frac{9}{2}\rangle$, where 3^- is the first excited state of the ^{208}Pb core. It would be possible to reproduce this effect by introducing a spin-independent $J=3$ component in \bar{G}' ; however, since we have no independent way of fixing the strength of this component a more reasonable approach would be to introduce these admixtures explicitly. This has been done elsewhere¹⁷ and a reasonable description of the (p, p') cross sections for this transition has been obtained. In these calculations it was necessary to include both the contribution from these low-lying particle-vibration admixtures and the contribution due to admixtures of states formed from higher-lying 3^- core excitations. The results shown in Tables VII and VIII for the $1h_{9/2} \rightarrow 1i_{13/2}$ transition are representative of the latter contribution only.

A previous estimate of the (p, p') cross section for the $1h_{9/2} \rightarrow 2f_{7/2}$ transition in ^{209}Bi has also been made.¹⁷ The first order wave functions of this work were used in this calculation. The calculations predicted important contributions to the cross section from all allowed $J0J$ amplitudes. This result was found to be consistent with the experimental data. An estimate of the modifica-

tion of the first order results due to the addition of contributions from low-lying particle-vibration admixtures was also made. Specifically, contributions from the particle-vibration states formed from the first 2^+ , 4^+ , 6^+ , and 8^+ excitations of the ^{208}Pb core were introduced. With these contributions, the first order ϵ_p^{J0J} were increased to $\epsilon_p^{202} = 6.94$, $\epsilon_p^{404} = 6.56$, $\epsilon_p^{606} = 5.17$, and $\epsilon_p^{808} = 4.03$. These values are in good agreement with the results we have obtained using \bar{G} as the core coupling interaction. This is another indication that the effect of core correlations can be reproduced by using a rather simple effective interaction in calculating \bar{V} .

$E2$ effective charges are known⁶⁴ for several transitions in the Pb region where there are no inelastic scattering data available. As an additional check on the consistency of our calculations we have calculated these effective charges. The results have been included in Table XI. The agreement between theory and experiment is quite good, with the possible exception of the result for the $1h_{9/2} \rightarrow 1h_{9/2}$ proton transition.

D. Cross sections and form factors

In this section we compare our theoretical (p, p') cross sections and (e, e') form factors directly

TABLE XII. Optical parameters used in the present calculations.

System ^a	E (MeV)	V (MeV)	r_0 (fm)	a (fm)	W (MeV)	W_D (MeV)	r'_0 (fm)	a' (fm)	V_s (MeV)	r_s (fm)	a_s (fm)
$^{42}\text{Ca} + p$ ^b	22.9	46.9	1.18	0.700	1.30	6.80	1.30	0.600	6.00	1.05	0.700
$^{50}\text{Ti} + p$ ^c	17.5	48.3	1.24	0.600	0.00	10.68	1.26	0.520	10.00	1.24	0.600
$^{50}\text{Ti} + p$ ^d	40.0	44.9	1.16	0.750	7.82	1.14	1.37	0.630	6.04	1.06	0.738
$^{83}\text{Y} + p$ ^e	18.9	52.6	1.20	0.700	0.00	9.80	1.25	0.650	5.70	1.20	0.700
$^{89}\text{Y} + p$ ^f	24.5	46.6	1.23	0.627	0.00	10.9	1.28	0.536	7.00	1.23	0.627
$^{89}\text{Y} + p$ ^g	61.2	39.5	1.20	0.693	5.12	2.54	1.40	0.534	6.92	1.00	0.861
$^{90}\text{Zr} + p$ ^h	18.8	52.0	1.20	0.700	0.00	9.25	1.25	0.650	6.20	1.20	0.700
$^{90}\text{Zr} + p$ ^g	61.2	39.5	1.20	0.693	5.12	2.54	1.40	0.534	6.92	1.00	0.861
$^{207}\text{Pb} + p$ ⁱ	20.2	53.0	1.25	0.650	0.00	10.0	1.25	0.760	6.00	1.20	0.470

^aWe write the optical potential

$$U = -V(1 + e^x)^{-1} - iW(1 + e^{x'})^{-1} + 4iW_D \frac{d}{dx'} (1 + e^{x'})^{-1} + (\hbar/m_\pi c)^2 V_s \frac{1}{r} \frac{d}{dr} (1 + e^{x_s})^{-1},$$

where

$$x = \frac{r - r_0 A^{1/3}}{a}, \quad x' = \frac{r - r'_0 A^{1/3}}{a'}, \quad x_s = \frac{r - r_s A^{1/3}}{a_s},$$

and to which is added the Coulomb potential of a uniformly charged sphere of radius $1.25A^{1/3}$.

^bSee Ref. 56.

^cSee Ref. 75.

^dSee Ref. 45.

^eSee Ref. 76.

^fSee Ref. 77.

^gSee Ref. 78.

^hSee Ref. 46.

ⁱSee Ref. 65.

TABLE XIII. Parameters for ground state proton distributions.

Nuclide ^a	ρ_0 (fm ⁻³)	c (fm)	a (fm)
⁴² Ca ^b	0.069	3.83	0.595
⁵⁰ Ti ^b	0.073	3.92	0.553
⁸⁸ Y ^c	0.073	4.80	0.568
⁹⁰ Zr ^c	0.074	4.85	0.568
²⁰⁷ Pb ^d	0.063	6.63	0.527

^aIt is assumed that the density distribution is given by $\rho_p(r) = \rho_0 \{1 + \exp[(r-c)/a]\}^{-1}$.

^bSee Ref. 54.

^cSee Ref. 79.

^dSee Ref. 80.

with experiment. The discussion will be brief since many of the important points have already been covered above. The optical model parameters used in the DWA calculations are summarized in Table XII. The ground state proton density parameters used in estimating the imaginary part of \bar{V} are summarized in Table XIII.

1. ⁴²Ca

The theoretical (p, p') cross sections for the excitation of the first 2^+ and 4^+ states in ⁴²Ca are compared with the 22.9 MeV experimental data of Ref. 56 in Fig. 6. The dotted curves $D(HJ)$ are the results obtained using only the real part of \bar{V} and the valence wave functions of Table II. The solid [$D + C(HJ)$] and dashed [$D + C(HJ) + Im$] curves are the results obtained with the transition densities of Table VIII using only the real part of \bar{V} and both the real and imaginary parts of \bar{V} , respectively. We do not show the results obtained with the transition densities of Table VII, because the differences between the calculations using G and \bar{G}' have been adequately discussed in the preceding section. The values of ϵ_p , shown in the figure are the square roots of the ratios of the $D + C(HJ)$ and $D(HJ)$ integrated cross sections. They differ somewhat from the values based on Eq. (101) and Eq. (103) which were given in Table VIII as expected. The value of ϵ_I provides a measure of the importance of the imaginary part of \bar{V} , i.e., ϵ_I^2 is the ratio of the $D + C(HJ + Im)$ and $D + C(HJ)$ integrated cross sections.

The agreement between experiment and the theoretical results with core polarization included is quite reasonable. We see clearly that the effect of core polarization decreases only slowly with increasing multipole. The theoretical cross sections obtained with the imaginary component of \bar{V} included in the calculations have slightly sharper structure than the cross sections obtained using

only the real part of \bar{V} . The shape of the experimental differential cross sections favor the former. We also note that the effect of the imaginary part of \bar{V} increases with increasing multipole.

The theoretical (e, e') form factor for the excitation of the first 2^+ state in ⁴²Ca is compared with the data of Ref. 65 in Fig. 7. In the calculation we have used the transition density of Table VIII. There is no valence form factor in this case, because the assumed model space consists only of neutron configurations. The theoretical result falls short of the data by about a factor of 3 as was pointed out previously. This deficiency in the theoretical wave functions does not show up in (p, p') results because neutron excitations are dominant there.

2. ⁵⁰Ti

The theoretical (p, p') cross sections for the excitation of the first 2^+ and 4^+ states in ⁵⁰Ti are compared with the 17.5 and 40.0 MeV data of Refs. 37 and 38 in Fig. 8. The format of the figure is the same as that of Fig. 6. With the exception of the values of ϵ_p , the results for ⁵⁰Ti have the same general characteristics as the results for ⁴²Ca. The increase in the values of

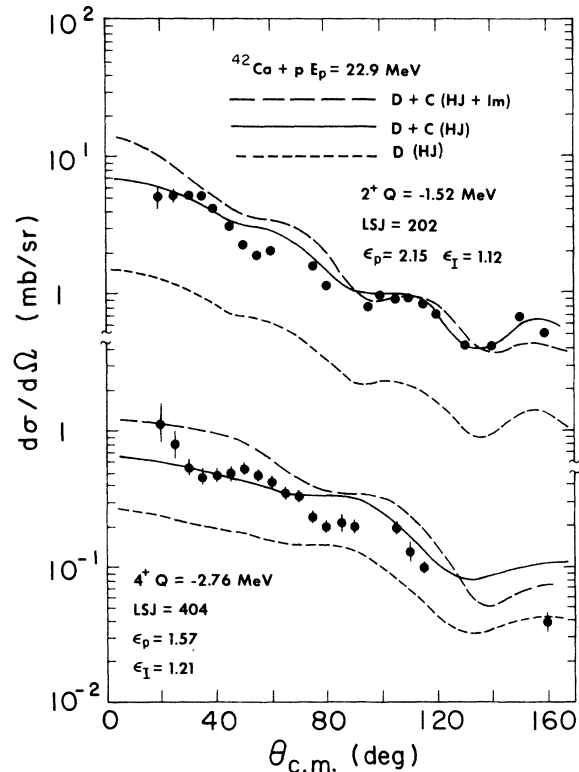


FIG. 6. Theoretical (p, p') cross sections for first 2^+ and 4^+ excitations in ⁴²Ca with $E_p = 22.9$ MeV.

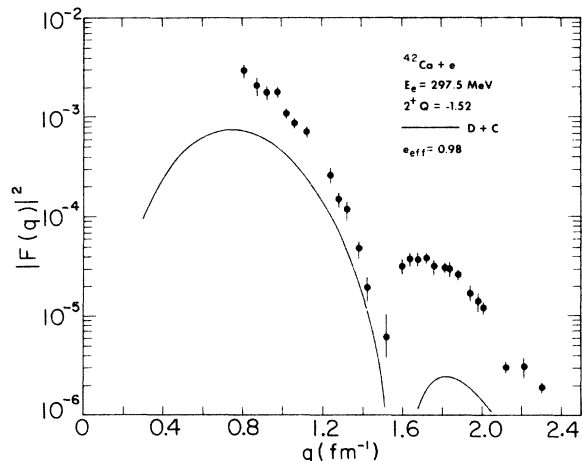


FIG. 7. Theoretical (e, e') form factor for first 2^+ state in ^{42}Ca .

ϵ_p for ^{50}Ti , compared with ^{42}Ca , is not due to an increase in the strength of core polarization in ^{50}Ti . It only reflects that the valence cross section $D(\text{HJ})$ for ^{50}Ti are smaller, because the model space includes only proton configurations in this case.

The theoretical (e, e') form factors for the excitation of the first 2^+ and 4^+ states in ^{50}Ti are compared with the data of Refs. 54 and 58 in Fig. 9. Here we have shown the results obtained using the wave function of Table II (D) and the transition densities of Table VIII ($D+C$). The results here show rather clearly the importance of $E4$ polarization.

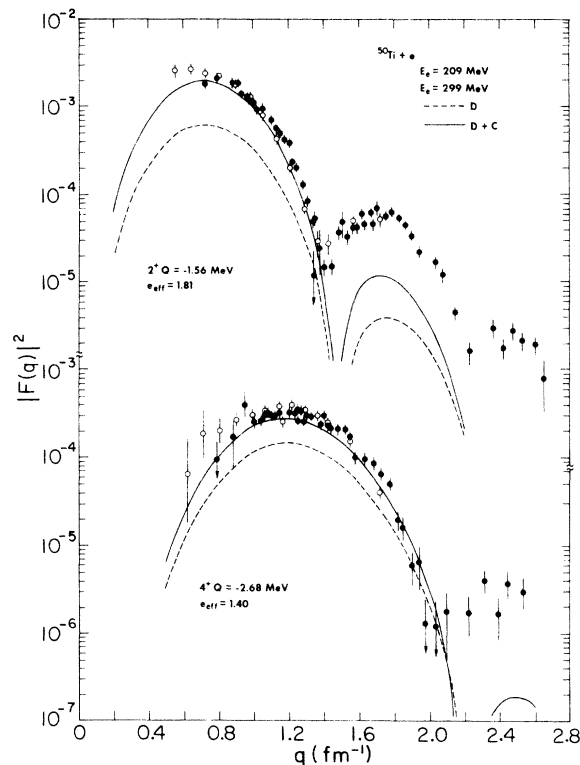


FIG. 9. Theoretical (e, e') form factors for first 2^+ and 4^+ states in ^{50}Ti .

3. ^{90}Zr

The theoretical (p, p') cross sections for the excitation of the first 2^+ , 4^+ , 6^+ , 8^+ , and 5^- states in ^{90}Zr are compared with the 18.8 and 61.2 MeV data of Refs. 39 and 43 in Figs. 10–12. The $LSJ = 515$ contribution to the 5^- cross section was

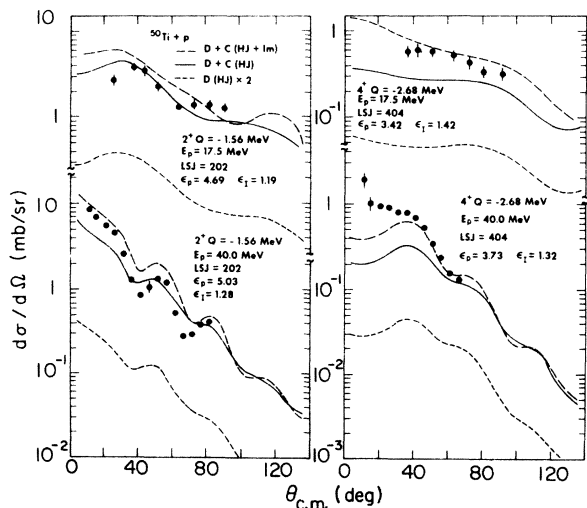


FIG. 8. Theoretical (p, p') cross sections for first 2^+ and 4^+ states in ^{50}Ti with $E_p = 17.5$ and 40.0 MeV.

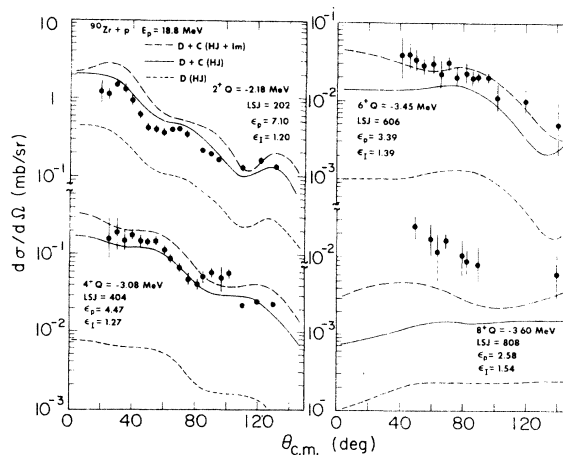


FIG. 10. Theoretical (p, p') cross sections for first 2^+ , 4^+ , 6^+ , and 8^+ excitations in ^{90}Zr with $E_p = 18.8$ MeV. Direct $LSJ = 202$ cross section has been multiplied by 10.

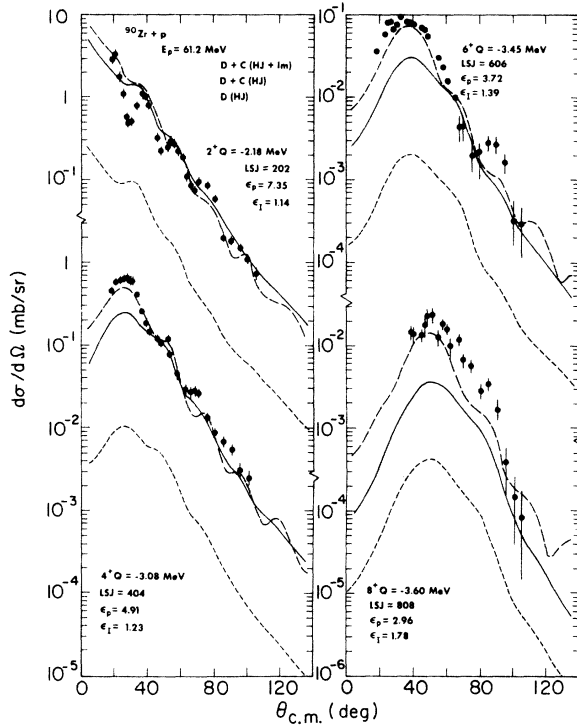


FIG. 11. Same as Fig. 10 with $E_p = 61.2$ MeV, except direct $LSJ=202$ cross section has been multiplied by 3.

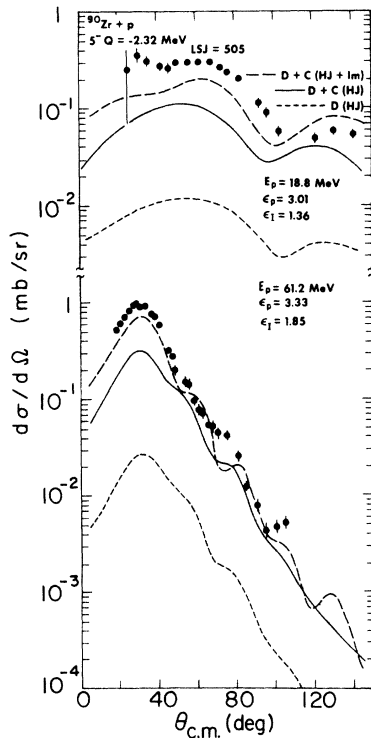


FIG. 12. Theoretical (p, p') cross sections for excitation of first 5^- level in ^{90}Zr at $E_p = 18.8$ and 61.2 MeV.

found to be negligible and has not been shown. Results for the excitation of these same levels by 40 MeV protons have previously been presented elsewhere.¹⁸

Again the overall agreement between experiment and the theoretical results with core polarization included is reasonable. Relative to the results for the 2^+ , 4^+ , and 6^+ excitations, the cross sections for the 8^+ and 5^- levels appear to be underestimated at 18.8 MeV. The situation is somewhat improved at 61.2 MeV. This improvement is also evident in the 40 MeV results. Collective model calculations^{18, 39, 43} for the 8^+ and 5^- excitations yield considerably larger values of β_L at 18.8 MeV than at 40 and 61.2 MeV. This is simply an indication that multiple excitation is important for these levels at the lower energies.

The imaginary part of \bar{V} is essential in reproducing the forward peaks of the 61.2 MeV cross sections for all of the excitations except the 2^+ level. It is also important in giving the correct multipole dependence for the theoretical cross sections. These same observations were made with respect to the 40 MeV results for these same excitations.¹⁸ These effects do not show up so clearly at 18.8 MeV partly because of the difficulty in reproducing the 8^+ and 5^- cross sections at this energy and partly because the shapes of the angular distributions are not so distinctive at the lower energies. The latter remark applies equally well to the 22.9 MeV results for ^{42}Ca and the 17.5 MeV results for ^{50}Ti . The effect of the imaginary part of \bar{V} is starting to show up in the results for ^{50}Ti at 40 MeV; however, the picture is not complete because of the limited range of multipoles which are available in this case.

The increasing importance of the imaginary part of \bar{V} with increasing multipole is a result of the zero-range form of t_{lp}^I , in contrast to the finite-range form of t_{lp}^R . The results we have obtained do not undeniably establish that the phenomenological treatment²⁰ of the imaginary part of \bar{V} is correct. We can conclude, however, that the multipole dependence obtained in the calculations using only the real part of \bar{V} is inadequate and it is interesting that the simple prescription for including the imaginary part of \bar{V} gives reasonable results.

Even with the imaginary part of \bar{V} included there are still some deficiencies in the 61.2 MeV results. These occur mainly at back angles where the $D+C(\text{HJ}+\text{Im})$ results have more structure than the data for the 2^+ , 4^+ , 6^+ , and 5^- excitations. In addition, the $D+C(\text{HJ}+\text{Im})$ results for the 8^+ state appears to underestimate the back angle cross section. It has been shown^{27, 43} that the inclusion of a spin-orbit component in \bar{V} can improve these

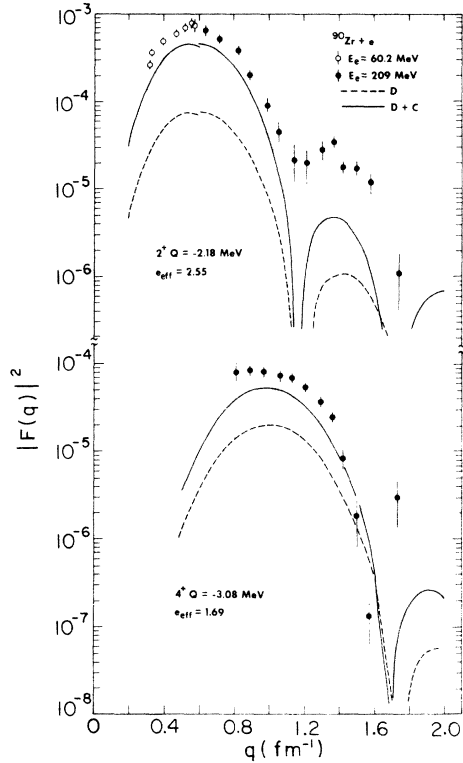


FIG. 13. Theoretical (e, e') form factors for first 2^+ and 4^+ excitations in ^{90}Zr .

results. In addition, the presence of contributions from this interaction component does provide some direct evidence of the decreasing importance of core correlations with increasing multipolarity.¹⁸

The theoretical (e, e') form factors for the excitation of the first 2^+ and 4^+ states in ^{90}Zr are compared with the experimental data of Refs. 58, 60, and 61 in Fig. 13. The format of the figure is the same as Fig. 9. Here again we have an example of important $E4$ polarization.

4. ^{89}Y

The theoretical (p, p') cross sections for the first $\frac{9}{2}^+$ excitation in ^{89}Y are compared with the 18.9, 24.5, and 61.2 MeV experimental cross sections of Refs. 76, 77, and 46 in Fig. 14. There are four allowed LSJ amplitudes for this transition. These are $LSJ = 314, 514, 505,$ and 515 . The contributions from the 514 and 515 amplitudes were found to be negligible. The 505 amplitude was found to be dominant, but the contribution from the 314 amplitude is appreciable, particularly at forward angles. This is consistent with the fact that the $\frac{9}{2}^+$ level in ^{89}Y is known to

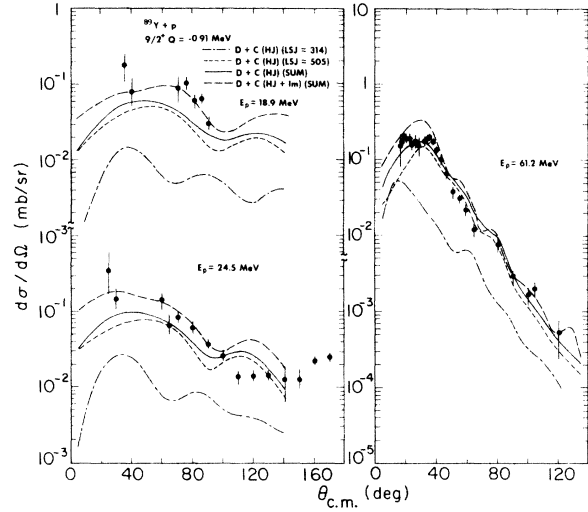


FIG. 14. Theoretical (p, p') cross sections for $2p_{1/2} \rightarrow 1g_{9/2}$ single proton transition in ^{89}Y with $E_p = 18.9, 24.5,$ and 61.2 MeV.

decay by $M4$ γ emission.⁸¹

In Fig. 14 we have shown the $LSJ = 314$ and 505 cross sections obtained using the real part of \bar{V} and the transition densities of Table VIII and IX. We have also shown the sum of these two cross sections. As before these curves are labeled $D+C(HJ)$. The valence results, $D(HJ)$, have not been shown. The fourth curve shown $D+C(HJ+Im)$ is the sum of the $LSJ = 314$ and 505 cross sections obtained using both the real and imaginary parts of V . For the $LSJ = 505$ cross section at 24.5 MeV, $\epsilon_p = 3.16$ and $\epsilon_t = 1.37$. At 18.9 and 61.2 MeV ϵ_p and ϵ_t for the $LSJ = 505$ cross section have the same values that were given in Fig. 12 for the excitation of the 5^- state in ^{90}Zr at these energies. (It is shown in the Appendix that the $LSJ = 505$ form factors for the $\frac{1}{2}^- \rightarrow \frac{9}{2}^+$ transition in ^{89}Y and the $0^+ \rightarrow 5^-$ transition in ^{90}Zr are essentially the same in our model.) For the $LSJ = 314$ cross sections, $\epsilon_p = 0.51, 0.52,$ and 0.50 at 18.9, 24.5, and 61.2 MeV. For this cross section $\epsilon_t = 1.0$ at all energies, because we have taken the imaginary part of \bar{V} to be spin independent.

From Fig. 14 we see that the theoretical calculations do not reproduce the energy dependence of the experimental cross sections exactly. The theoretical results are in good agreement with the data at the lower energies, but a bit too high at 61.2 MeV. A similar discrepancy was noted in the results for the 5^- level in ^{90}Zr , except that the theoretical results were a little low at 18.8 MeV and in fairly good agreement with the data at 61.2 MeV. There is a noticeable difference in shape, at forward angles, between the 61.2 MeV

experimental cross sections for the $\frac{9}{2}^+$ excitation in ^{89}Y and the 5^- excitation in ^{90}Zr . This is consistent with the presence of the $LSJ = 314$ contribution to the former. It appears that the $LSJ = 505$ contribution to the ^{89}Y cross section is slightly overestimated in our calculation, so this effect does not show up quite so clearly in our theoretical results. We conclude that the $LSJ = 505$ contribution to the cross section for the $\frac{9}{2}^+$ state in ^{89}Y is somewhat smaller than the corresponding contribution to the cross section for the 5^- state in ^{90}Zr , a feature which cannot be reproduced with the simple model for core polarization that we are using.

5. ^{207}Pb

The theoretical (p, p') cross sections for the excitation of the first four single particle states in ^{207}Pb are compared with the 20.2 MeV experimental data of Ref. 65 in Fig. 15. Results for the excitation of these same levels at 39.5 MeV have previously been presented elsewhere.⁴⁶ Contributions from $S=1$ amplitudes were found to be negligible in all cases and only $S=0$ contributions to the cross sections are shown in the figure. There are two interesting aspects to the results. One is that ϵ_p for the $\frac{7}{2}^-$ excitation which goes by $LSJ = 404$ transfer is comparable to ϵ_p for the $\frac{5}{2}^-$ and $\frac{3}{2}^-$ excitations which proceed with $LSJ = 202$ transfer. Other evidence for large $L=4$ core polarization in the Pb region was seen previously in the cross section for the excitation of the $2f_{7/2}$ single particle state in ^{209}Bi by 61.2 MeV protons.¹⁷ The other interesting feature is that there is a shape difference between the cross section for the $\frac{3}{2}^-$ level and $\frac{5}{2}^-$ level both of which are excited by $LSJ = 202$ transfer. Although the theoretical results do not give a completely accurate reproduction of the experimental data, they do show this shape difference rather nicely. The difference in shapes is due to the differences in the radial wave functions for the valence neutrons in the two final states. Similar effects are not seen in the lighter nuclei, because the radial wave functions tend to be more similar there, at least for the cases we have considered.

6. ^{209}Bi

Theoretical (p, p') cross sections for states in ^{209}Bi obtained using the wave functions of this work have been discussed in detail elsewhere¹⁷ and will not be discussed here.

V. CONCLUSIONS

We have shown that a fair sized sampling of experimental inelastic electron and proton scatter-

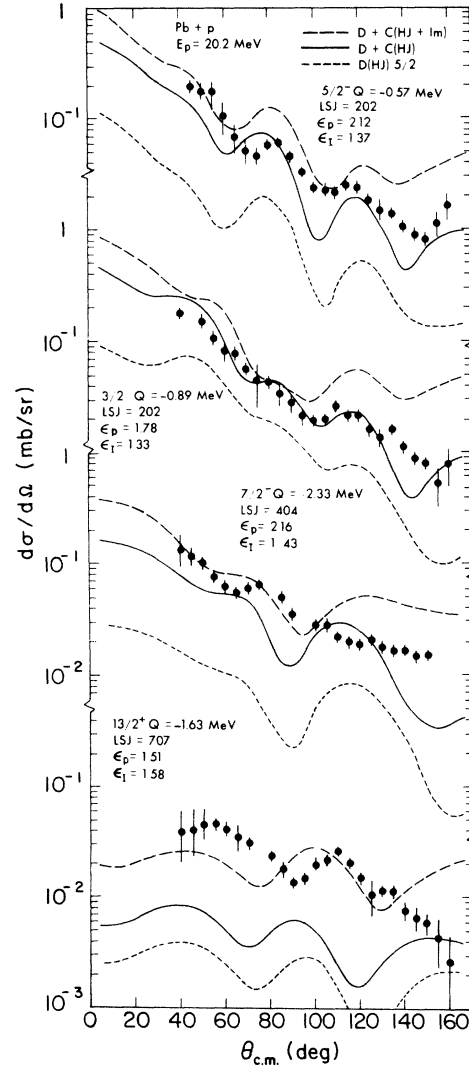


FIG. 15. Theoretical (p, p') cross sections for neutron hole transitions in ^{207}Pb with $E_p = 20.2$ MeV.

ing data for nuclei near closed shells can be understood, at least qualitatively, in calculations which assume to a first approximation that the interaction between two bound nucleons and between a bound and a continuum nucleon are given by G matrix interactions derived from free two-nucleon potentials. In the calculations, the (e, e') reaction was treated using a modified Born approximation. The (p, p') reaction was treated using the distorted-wave approximation and the G matrix interaction was modified to account for knock-on exchange and excluded reaction channels. Core polarization was treated in lowest order and with the G matrix interaction renormalized to roughly account for the effect of long-range core correlations. The results clearly

show that core polarization effects are large and persist as the multipolarity of the transitions increase. They also show that the motions of target protons and neutrons are strongly correlated although there may be some weakening in the correlation for transitions where the L transfer exceeds 5.

Although our results indicate a strong correlation between proton and neutron motions in the excitation of the levels considered, in detail there are small differences between proton and neutron motions even for the $L=2$ transitions. Brown and Madsen⁸² have recently discussed some of the expected differences and it would surely be interesting to examine our results more carefully in this regard. This can, in principle, be done on the basis of the data we have considered,¹⁴ but it requires considerably greater care in the calculations than we have expended and thus must be postponed until a later date. Forthcoming data⁸³ for the excitation of nuclear levels by π^+ and π^- inelastic scattering should provide additional information concerning these differences.

Finally we note that the use of an "effective" core coupling interaction in a first order treatment of the renormalization of one-body operators was found to give reasonable results in the sense that it does seem to account for some of the effects attributable to collective correlations in the core. It would be interesting to pursue this further taking care to include the second order terms that we have ignored. Other interaction choices might also be investigated, for example the recent effective interaction of Schiffer and True.⁸⁴

One of us (F. P.) would like to thank the staffs of the Michigan State University Cyclotron Laboratory and the Lawrence Berkeley Laboratory for their assistance during the course of this work.

APPENDIX

In this Appendix we give the values of the spectroscopic amplitudes S_q^J for the specific transitions we are considering. S_q^J is defined in Eq. (71).

$$\langle n_f l_f j_f^{-1} \| \bar{T}^{LSJ} \| n_i l_i j_i^{-1} \rangle = -(-1)^S \left\{ \langle j_f \| t_q^{LSJ} \| j_i \rangle + \sum_{j_p j_h} \left[\frac{1}{Q - \epsilon(\text{ph})} P_{\text{ph}} + \frac{1}{-Q - \epsilon(\text{ph})} \right] F_{q\alpha'}^J(j_p j_h, j_f j_i) \right\}. \quad (\text{A8})$$

The matrix elements for a single hole transition differ from the matrix elements for a single particle transition by an overall phase which depends on the particular operator being considered. This is of no consequence in this work because we are only interested in the square of these matrix elements. Another difference is that the position of P_{ph} has been shifted from the second to the first term inside the brackets. This has nearly a negligible effect because $\epsilon(\text{ph})$ is typically much greater than Q and the effect of P_{ph} on $F_{q\alpha'}^J$ is weak as may be seen from Eq. (87) which is valid for the case of a zero-range coupling interaction.

A. Single particle transitions

For a transition between two single particle states,

$$| \alpha_i(n) J_i M_i \rangle \equiv | n_i l_i j_i m_i \rangle = a_i^\dagger | C \rangle, \quad (\text{A1})$$

$$| \alpha_f(n) J_f M_f \rangle \equiv | n_f l_f j_f m_f \rangle = a_f^\dagger | C \rangle, \quad (\text{A2})$$

Eq. (74) gives

$$S_q^J(n_f l_f j_f, n_i l_i j_i; j_\alpha j_\gamma) = \delta_{j_i j_\gamma} \delta_{j_f j_\alpha}. \quad (\text{A3})$$

Inserting this result in Eq. (80) we obtain [see Eq. (A8)]:

$$\begin{aligned} \langle n_f l_f j_f \| \bar{T}^{LSJ} \| n_i l_i j_i \rangle &= \langle j_f \| t_q^{LSJ} \| j_i \rangle \\ &+ \sum_{j_p j_h} \left[\frac{1}{Q - \epsilon(\text{ph})} + \frac{1}{-Q - \epsilon(\text{ph})} P_{\text{ph}} \right] \\ &\times F_{q\alpha'}^J(j_p j_h, j_f j_i), \quad (\text{A4}) \end{aligned}$$

where Q and $\epsilon(\text{ph})$ have been defined in Eq. (91).

B. Single hole transition

For a transition between two single hole states,

$$\begin{aligned} | \alpha_i(n) J_i M_i \rangle &\equiv | n_i l_i j_i^{-1}, -m_i \rangle \\ &= (-1)^{j_i - m_i} a_i | C \rangle, \quad (\text{A5}) \end{aligned}$$

$$\begin{aligned} | \alpha_f(n) J_f M_f \rangle &\equiv | n_f l_f j_f^{-1}, -m_f \rangle \\ &= (-1)^{j_f - m_f} a_f | C \rangle, \quad (\text{A6}) \end{aligned}$$

Eq. (74) gives

$$\begin{aligned} S_q^J(n_f l_f j_f^{-1}, n_i l_i j_i^{-1}; j_\alpha j_\gamma) &= (-1)^{j_i + j_f - j_\alpha - j_\gamma} \hat{j}_i \hat{j}_f^{-1} \delta_{j_i j_\alpha} \delta_{j_f j_\gamma}. \quad (\text{A7}) \end{aligned}$$

Inserting this result in Eq. (80) and then making use of the conjugation relation Eq. (78) and the permutation property of $F_{q\alpha'}^J$, given in Eq. (82), we find

We conclude that single particle transitions and single hole transitions are equivalent for all practical purposes.

C. Transitions between two particle states

For a transition between two particle states,

$$|\alpha_i(n)J_i M_i\rangle \equiv |(jj_1)J_i M_i\rangle = \sum_{mm_1} \langle jj_1 mm_1 | J_i M_i \rangle a_1^\dagger a_1^\dagger | C \rangle, \quad (\text{A9})$$

$$|\alpha_f(n)J_f M_f\rangle \equiv |(jj_2)J_f M_f\rangle = \sum_{mm_2} \langle jj_2 mm_2 | J_f M_f \rangle a_2^\dagger a_2^\dagger | C \rangle, \quad (\text{A10})$$

the spectroscopic amplitude is given by

$$\begin{aligned} S_q^J((jj_2)J_f, (jj_1)J_i; j_\alpha j_\gamma) &= (1 + \delta_{jj_1})^{-1/2} (1 + \delta_{jj_2})^{-1/2} (-1)^{j_1 + j_2 + J_f} \hat{J}_i \\ &\times \left([1 + (-1)^{j_1} \delta_{jj_1} + (-1)^{j_2} \delta_{jj_2}] \delta_{j_\alpha j_2} \delta_{j_\gamma j_1} (-1)^{j_2} \hat{J}_2 \left\{ \begin{matrix} j & j_1 & J_i \\ J & J_f & j_2 \end{matrix} \right\} \right. \\ &\left. + \delta_{j_1 j_2} \delta_{j_2 j_\alpha} \delta_{j_\gamma j_1} (-1)^{j_1} \hat{J}_1 \left\{ \begin{matrix} j & j & J_i \\ J & J_f & j \end{matrix} \right\} \right). \end{aligned} \quad (\text{A11})$$

In the special case $j_1 = j_2 = j$, J_i and J_f must be even and Eq. (A11) reduces to

$$S_q^J((j^2)J_f, (j^2)J_i; j_\alpha j_\gamma) = -\delta_{j_\alpha j_\gamma} \delta_{j_\alpha j_\gamma} (-1)^{j_2} \hat{J}_i \hat{J}_1 \left\{ \begin{matrix} j & j & J_i \\ J & J_f & j \end{matrix} \right\}. \quad (\text{A12})$$

For this case we find

$$\langle (j^2)J_f \| \bar{T}^{LSJ} \| (j^2)J_i \rangle = -(-1)^{j_2} \hat{J}_i \hat{J}_1 \left\{ \begin{matrix} j & j & J_i \\ J & J_f & j \end{matrix} \right\} \left\{ \begin{matrix} j \\ j \end{matrix} \| t_q^{LSJ} \| j \right\} + \sum_{j_p j_h} \left[-\frac{1}{\epsilon(\text{ph})} (1 + (-1)^{S+J}) \right] F_{qq'}^J(j_p j_h, jj), \quad (\text{A13})$$

where we have again used Eq. (82). It is interesting to note that when $J_i = 0$, then $J = J_f$ is even, and the second term on the right hand side of Eq. (A13) vanishes when $S = 1$. The valence contribution given by the first term on the right of Eq. (A13) vanishes in this case also; so, core polarization does not break the valence selection rule. When $J_i = 0$ and $S = 0$, the factor in parentheses in the curly brackets becomes 2 and core polarization is effective.

Another case of particular interest here is the transition between the states

$$|\alpha_i(n)J_i M_i\rangle = a | (j_1^2)J_i = 0 M_i = 0 \rangle + b | (j_2^2)J_i = 0 M_i = 0 \rangle, \quad (\text{A14})$$

$$|\alpha_f(n)J_f M_f\rangle = | (j_2 j_1)J_f M_f \rangle. \quad (\text{A15})$$

This corresponds to the description of the $0^+ \rightarrow 5^-$ transition in ^{90}Zr given in Table II. In this case we find

$$S_q^J(\alpha_f J_f, \alpha_i J_i; j_\alpha j_\gamma) = \sqrt{2} \hat{J}_f^{-1} [a \hat{J}_2 \hat{J}_1^{-1} \delta_{j_\alpha j_2} \delta_{j_\gamma j_1} - (-1)^{j_1 + j_2 - J_f} b \hat{J}_1 \hat{J}_2^{-1} \delta_{j_\alpha j_1} \delta_{j_\gamma j_2}]. \quad (\text{A16})$$

Inserting this expression into Eq. (80) and again making use of Eq. (78) and Eq. (82), we obtain

$$\begin{aligned} \langle \alpha_f J_f \| \bar{T}^{LSJ} \| \alpha_i J_i \rangle &= \sqrt{2} \hat{J}_f^{-1} [a \hat{J}_2 \hat{J}_1^{-1} + (-1)^S b] \left\{ \left\langle j_2 \right\| t_q^{LSJ} \left\| j_1 \right\rangle + \sum_{j_p j_h} \left[\frac{1}{\epsilon(12) - \epsilon(\text{ph})} + \frac{1}{\epsilon(21) - \epsilon(\text{ph})} P^{\text{ph}} \right] \right. \\ &\left. \times F_{qq'}^J(j_p j_h, j_2 j_1) \right\}. \end{aligned} \quad (\text{A17})$$

These expressions differ from those for the single particle transition $j_1 \rightarrow j_2$ only by an overall constant. With $j_1 = 2p_{1/2}$, $j_2 = 1g_{9/2}$, $a = 0.8$, $b = 0.6$, $J_f = 5$, and $S = 0$, this constant has the value 1.02. With $S = 1$ the constant is 0.507. We conclude that the important $LSJ = 505$ amplitude for the $0^+ \rightarrow 5^-$ transition in ^{90}Zr is nearly identical to the corresponding amplitude for the $2p_{1/2} \rightarrow 1g_{9/2}$ transition in ^{89}Y . The $LSJ = 515$ amplitude for the ^{90}Zr transition is reduced in magnitude in comparison to corresponding amplitude for the ^{89}Y transition.

- *Work supported in part by the U.S. Energy Research and Development Administration and N.S.F. Grants Nos. NSF-PHY-74-18194 AO1 and NSF-PHY-74-02673.
- †Permanent address: Department of Physics, The Florida State University, Tallahassee, Florida 32306.
- ¹L. L. Foldy and J. T. Milford, *Phys. Rev.* **80**, 751 (1950); A. Bohr and B. Mottelson, *K. Dan. Vidensk. Selsk. Mat.-Fys. Medd* **27**, 16 (1953); A. Kerman, *Phys. Rev.* **92**, 1176 (1953); K. W. Ford and C. A. Levinson, *ibid.* **100**, 1 (1955); R. D. Amado, *ibid.* **108**, 1462 (1957).
- ²R. J. Blin-Stoyle, *Proc. Phys. Soc.* **A66**, 1158 (1953); R. J. Blin-Stoyle and M. A. Perks, *ibid.* **A67**, 885 (1954); A. Arima and H. Horie, *Progr. Theor. Phys.* **11**, 509 (1954); **12**, 623 (1954); H. Horie and A. Arima, *Phys. Rev.* **99**, 778 (1955); A. de-Shalit, *ibid.* **113**, 547 (1959).
- ³G. F. Bertsch, *Nucl. Phys.* **74**, 234 (1965).
- ⁴T. T. S. Kuo and G. E. Brown, *Nucl. Phys.* **85**, 40 (1966).
- ⁵G. E. Brown, *Unified Theory of Nuclear Models and Nucleon-Nucleon Forces*, (North-Holland, Amsterdam, 1967), 2nd ed.
- ⁶M. H. MacFarlane, *Nuclear Structure and Nuclear Reactions, Proceedings of the International School of Physics "Enrico Fermi," Course XL*, 1967 (Academic, New York, 1969), p. 457.
- ⁷Other works cited in Refs. 3-6.
- ⁸T. T. S. Kuo, *Nucl. Phys.* **A90**, 199 (1967); **A103**, 71 (1967); G. E. Brown and T. T. S. Kuo, *ibid.* **A92**, 481 (1967); T. T. S. Kuo and G. E. Brown, *ibid.* **A114**, 241 (1968); T. T. S. Kuo and G. Herling, *ibid.* **A181**, 113 (1972).
- ⁹B. R. Barrett and M. W. Kirson, *Phys. Lett.* **27B**, 544 (1968); **30B**, 8 (1969); *Nucl. Phys.* **A148**, 145 (1970); M. W. Kirson, *Ann. Phys. (N.Y.)* **66**, 624 (1971).
- ¹⁰J. Blomqvist, N. Freed, and H. O. Zetterstrom, *Phys. Lett.* **18**, 47 (1965); H. A. Mavromatis and L. Zamick, *Nucl. Phys.* **A104**, 17 (1967); J. D. Vergados, *Phys. Lett.* **36B**, 12 (1971); A. Arima and L. J. Huang-Lin, *ibid.* **41B**, 429, 435; P. Federman and L. Zamick, *Phys. Rev.* **177**, 1534 (1969); S. Siegal and L. Zamick, *Phys. Lett.* **28B**, 450, 453, (1969); *Nucl. Phys.* **A145**, 89 (1970).
- ¹¹B. R. Barrett and M. W. Kirson, *Adv. Nucl. Phys.* **6**, 219 (1973).
- ¹²F. Petrovich, H. McManus, V. Madsen, and J. Atkinson, *Phys. Rev. Lett.* **22**, 895 (1969); K. H. Bray *et al.*, *Nucl. Phys.* **A189**, 35 (1972); D. Slanina and H. McManus, *ibid.* **A116**, 271 (1968).
- ¹³G. R. Satchler, *Comment Nucl. Part. Phys.* **5**, 39 (1972), and references contained therein.
- ¹⁴G. R. Hammerstein, R. H. Howell, and F. Petrovich, *Nucl. Phys.* **A213**, 45 (1973).
- ¹⁵W. G. Love and G. R. Satchler, *Nucl. Phys.* **A101**, 424 (1967).
- ¹⁶D. Agassi and R. Schaeffer, *Nucl. Phys.* **A145**, 401 (1970).
- ¹⁷W. Benenson, S. M. Austin, P. J. Locard, F. Petrovich, J. Borysowicz, and H. McManus, *Phys. Rev. Lett.* **24**, 901 (1970); A. Scott, M. Owais, and F. Petrovich, *Nucl. Phys.* **A226**, 109 (1974).
- ¹⁸R. A. Hinrichs, D. Larson, B. M. Preedom, W. G. Love, and F. Petrovich, *Phys. Rev. C* **7**, 1981 (1973).
- ¹⁹N. Vinh-Mau, in *Theory of Nuclear Structure*, Trieste lectures, 1969 (IAEA, Vienna, 1970).
- ²⁰G. R. Satchler, *Phys. Lett.* **35B**, 279 (1971).
- ²¹R. H. Howell and G. R. Hammerstein, *Nucl. Phys.* **A192**, 651 (1972).
- ²²K. A. Amos, V. A. Madsen, and I. E. McCarthy, *Nucl. Phys.* **A94**, 103 (1967); J. Atkinson and V. A. Madsen, *Phys. Lett.* **21**, 295 (1968); *Phys. Rev. C* **1**, 1377 (1970).
- ²³D. Agassi and R. Schaeffer, *Phys. Lett.* **26B**, 703 (1968); R. Schaeffer, *Nucl. Phys.* **A132**, 186 (1969); Ph.D. thesis, Orsay 1969 (unpublished).
- ²⁴W. G. Love, *Particles and Nuclei* **3**, 318 (1972).
- ²⁵T. Hamada and I. D. Johnston, *Nucl. Phys.* **34**, 382 (1962).
- ²⁶J. Raynal, in *Symposium sur les Mechanismes de Réactions Nucléaires et phénomènes de Polarisation*, Université Laval, Quebec, 1969 (unpublished).
- ²⁷W. G. Love, *Phys. Lett.* **35B**, 371 (1971); *Nucl. Phys.* **A192**, 49 (1972); W. G. Love, and L. J. Parish, *Nucl. Phys.* **A157**, 625 (1970).
- ²⁸Glendenning (see Ref. 6), p. 332.
- ²⁹N. K. Glendenning and M. Veneroni, *Phys. Rev.* **144** 839 (1966); G. R. Satchler, *Nucl. Phys.* **77**, 481 (1966); V. A. Madsen, *ibid.* **80**, 177 (1966).
- ³⁰D. M. Brink and G. R. Satchler, *Angular Momentum* (Oxford U.P., Oxford, 1962).
- ³¹T. deForest, Jr., and J. D. Walecka, *Advan. Phys.* **15**, 1 (1966).
- ³²T. Janssens, J. Hofstadter, E. B. Hughes, and M. R. Yearian, *Phys. Rev.* **124**, B922 (1966).
- ³³G. R. Satchler, *J. Math. Phys.* **13**, 1118 (1972).
- ³⁴M. Harvey and F. C. Khanna, *Nucl. Phys.* **A152**, 588 (1970); **A155**, 337 (1970).
- ³⁵G. R. Satchler and W. G. Love, *Nucl. Phys.* **A172**, 449 (1971).
- ³⁶T. T. S. Kuo (unpublished).
- ³⁷H. O. Funsten, N. R. Roberson, and E. Rost, *Phys. Rev.* **134**, 117B (1964).
- ³⁸B. M. Preedom, C. R. Gruhn, T. Y. T. Kuo, and C. J. Maggiore, *Phys. Rev. C* **2**, 166 (1970).
- ³⁹W. S. Gray, R. A. Kenefick, J. J. Kraushaar, and B. W. Ridley, *Phys. Rev.* **142**, 735 (1966).
- ⁴⁰F. Petrovich and H. McManus, *Bull. Am. Phys. Soc.* **13**, 631 (1968).
- ⁴¹G. A. Peterson, K. Hosoyama, M. Nagao, A. Nakado, and Y. Torizuka, *Phys. Rev. C* **7**, 1028 (1973).
- ⁴²See, for example, V. Gillet, and N. Vinh Mau, *Nucl. Phys.* **54**, 321 (1964).
- ⁴³M. L. Whiten, A. Scott, and G. R. Satchler, *Nucl. Phys.* **A181**, 417 (1972).
- ⁴⁴A. Scott, M. Owais, and W. G. Love, *Nucl. Phys.* (to be published).
- ⁴⁵M. Owais, A. Scott, and W. G. Love (unpublished).
- ⁴⁶W. T. Wagner, G. R. Hammerstein, G. M. Crawley, J. Borysowicz, and F. Petrovich, Lawrence Berkeley Laboratory Report No. LBL-1938 (unpublished); *Phys. Rev. C* **7**, 1981 (1973).
- ⁴⁷B. R. Mottleson, *J. Phys. Soc. Jpn. Suppl.* **24**, 96 (1968); I. Hamamoto, *Nucl. Phys.* **A126**, 545 (1969); N. Auerbach and N. Stein, *Phys. Lett.* **28B**, 628 (1969); R. Broglia, J. Damgaard, and M. Molinari, *Nucl. Phys.* **A127**, 429 (1969).
- ⁴⁸F. Petrovich, *Nucl. Phys.* **A203**, 65 (1972).
- ⁴⁹A. Kallio and K. Koltveit, *Nucl. Phys.* **53**, 87 (1964).
- ⁵⁰S. G. Nilsson, *K. Dan. Vidensk. Selsk. Mat.-Fys.*

- Medd. 29, 16 (1955).
- ⁵¹J. H. E. Mattauch, W. Thiele, and A. H. Wapstra, Nucl. Phys. 67, 1 (1965).
- ⁵²R. H. Trilling (private communication).
- ⁵³D. A. Bromley and J. Weneser, Comments Nucl. Part. Phys. 11, 121 (1968).
- ⁵⁴J. Heisenberg, J. S. McCarthy, and I. Sick, Nucl. Phys. A164, 353 (1971).
- ⁵⁵A. M. Bernstein, E. P. Lippincott, G. T. Sample, and C. B. Thorn, Nucl. Phys. A115, 79 (1968).
- ⁵⁶J. C. Bane, J. J. Kraushaar, B. W. Ridley, and M. M. Stautberg, Nucl. Phys. A116, 580 (1968).
- ⁵⁷H. J. Eramuspe, Nucl. Phys. A101, 138 (1967).
- ⁵⁸Phan-Xuan-Ho, J. Bellicard, Ph. Leconte, and I. Sick, Nucl. Phys. A210, 189 (1973).
- ⁵⁹J. Vervier, Phys. Lett. 13, 47 (1964).
- ⁶⁰J. Bellicard, Ph. Leconte, T. H. Curtiss, R. A. Eisenstein, D. W. Madsen, and C. Bockleman, Nucl. Phys. A143, 213 (1970).
- ⁶¹M. Mills, Ph.D. thesis, Massachusetts Institute of Technology, 1972 (unpublished).
- ⁶²R. T. Wagner, E. R. Schunk, and R. B. Day, Phys. Rev. 130, 1962 (1962).
- ⁶³H. H. Landolt and R. Bernstein, in *Energy Levels in Nuclei*, edited by A. M. Hellwege and K. H. Hellwege (Springer, Berlin, 1961).
- ⁶⁴G. Astner, J. Bergström, J. Blomqvist, B. Fant, and K. Wikström, Nucl. Phys. A182, 219 (1972).
- ⁶⁵C. Glashausser, B. G. Harvey, D. L. Hendrie, J. Mahoney, E. A. McClatchie, and J. Saudinos, Phys. Rev. Lett. 21, 918 (1968).
- ⁶⁶J. W. Hertel, D. G. Fleming, J. P. Schiffer, and H. E. Gove, Phys. Rev. Lett. 23, 448 (1969).
- ⁶⁷R. A. Broglia, J. S. Lilley, R. Perazzo, and W. R. Phillips, Phys. Rev. C 1, 1508 (1970).
- ⁶⁸J. F. Ziegler and G. A. Peterson, Phys. Rev. 165, 1337 (1968).
- ⁶⁹R. H. Bassel, G. R. Satchler, R. M. Drisko, and E. Rost, Phys. Rev. 128, 2293 (1962).
- ⁷⁰G. R. Hammerstein, D. Larson, and B. H. Wildenthal, Phys. Lett. 39B, 176 (1972).
- ⁷¹J. Blomqvist and S. Wahlborn, Ark. Fys. 16, 545 (1960).
- ⁷²T. Nomura, C. Gil, H. Saito, and T. Yamazaki, Phys. Rev. Lett. 25, 1342 (1970).
- ⁷³B. H. Flowers and L. D. Skouras, Nucl. Phys. A116, 529 (1968).
- ⁷⁴W. J. Courtney and H. T. Fortune, Phys. Lett. 41B, 4 (1972).
- ⁷⁵R. J. Peterson, Ann. Phys. (N.Y.) 53, 40 (1969).
- ⁷⁶M. M. Stautberg, J. J. Kraushaar, and B. W. Ridley, Phys. Rev. 157, 977 (1967).
- ⁷⁷W. Benenson, S. M. Austin, R. A. Paddock, and W. G. Love, Phys. Rev. 176, 1268 (1968).
- ⁷⁸C. B. Fulmer, J. B. Ball, A. Scott, and M. L. Whiten, Phys. Rev. 181, 1565 (1969).
- ⁷⁹R. H. Helm, Phys. Rev. 104, 1466 (1956); G. A. Peterson and J. Alster, *ibid.* 166, 1136 (1967).
- ⁸⁰J. F. Ziegler and G. A. Peterson, Phys. Rev. 165, 1337 (1968).
- ⁸¹M. Goldhaber and A. W. Sunyar, Phys. Rev. 83, 906 (1951).
- ⁸²V. R. Brown and V. A. Madsen, Phys. Rev. C 11, 1298 (1975).
- ⁸³H. O. Funsten, W. J. Kossler, B. J. Lieb, H. S. Plendl, C. E. Stronach, and V. G. Lind (unpublished).
- ⁸⁴J. P. Schiffer and W. W. True, Rev. Mod. Phys. 48, 191 (1976).